PAPER

Crown-linked dipyridylamino-triazine ligands and their spin-crossover iron(ii) derivatives: magnetism, photomagnetism and cooperativity†

Hayley S. Scott,[a] Tamsyn M. Ross,[a] Nicholas F. Chilton,[a,b] Ian A. Gass,[a] Boujemaa Moubaraki,[a] Guillaume Chastanet,[c] Nicolas Paradis,[c] Jean-François Lètard,[c] Kuduva R. Vignesh,[d] Gopalan Rajaraman,[d] Stuart R. Batten[a] and Keith S. Murray*[a]

The syntheses, crystallography and magnetic properties of a series of compounds of formula *trans*-[$Fe^{II}(L^1)_2(NCX)_2$] (X = S, Se, BH_3 (**1–3**)), *cis*-[$Fe^{II}(L^2)(NCX)_2$]·CH_2Cl_2 (X = S, Se, BH_3 (**4–6**)) and *trans*-[$Fe^{II}(L^3)$-$(NCX)_2]_n$ (X = S, Se (**7–8**)) are described (L^1 = 6-chloro-N^2,N^2-diethyl-N^4,N^4-di(pyridin-2-yl)-1,3,5-triazine-2,4-diamine, L^2 = 6,6′-(1,4,10,13-tetraoxa-7,16-diazacyclooctadecane-7,16-diyl)bis(N^2,N^2-diethyl-N^4,N^4-di-(pyridin-2-yl)-1,3,5-triazine-2,4-diamine, L^3 = 6,6′-(1,4,10,13-tetraoxa-7,16-diazacyclooctadecane-7,16-diyl)bis(N^2,N^2,N^4,N^4-tetra(pyridin-2-yl)-1,3,5-triazine-2,4-diamine)). The magnetostructural properties of **1–8** have been probed in detail by variable temperature magnetic measurements and crystallographic methods. **1–6** display mononuclear structures while **7** and **8** form 1-D chain structures. Complexes **4–6** have the potential to form 1D-chains *via* L^2 bridging, but instead form mononuclear complexes. Magnetic studies show that complexes **1**, **2**, and **4** remain in the high-spin (HS) state at all temperatures. An aged, dry, powdered sample of **3** gives an abrupt HS to LS transition ($T_{1/2}$ = 200 K), while a freshly prepared, powdered sample of **3**·1.5H_2O displays thermal hysteresis (Δ = 7 K). Complexes **5**, **6** and **7** undergo a gradual spin transition with $T_{1/2}$ values of 100 K, 150 K and 130 K, respectively. Cooperativity parameters are compared, with **3** showing cooperativity (positive *C*) and **5** and **6** showing anticooperativity. Photomagnetic LIESST (light induced excited spin state trapping) studies were performed on complexes **5** and **6** and reveal *T*(LIESST) values lower than 60 K. An attempt has been made to understand the electronic structure of complex **3** and its cooperativity behaviour using density functional methods, the calculations reproducing the sign and, in part, the magnitude of the cooperativity.

Introduction

Spin crossover (SCO) materials[1] have the property of molecular bistability, in that they can exist in two different electronic states at a particular temperature. A growing number of SCO

[a]School of Chemistry, Building 23, Monash University, Clayton, Victoria 3800, Australia. E-mail: keith.murray@monash.edu; Fax: +61-3-99054597; Tel: +61-3-99054512

[b]School of Chemistry, University of Manchester, Oxford Road, Manchester, M13 9PL, UK

[c]CNRS, Université de Bordeaux, ICMCB, 87 avenue du Dr. A. Schweitzer, 33608 Pessac, France

[d]Department of Chemistry, IITB, Powai, Mumbai, 400076, India

†Electronic supplementary information (ESI) available: Figures of molecular structures and intermolecular contacts. Figures of Slichter–Drickamer fits. Figures of photomagnetism and reflectivity for **5** and thermal magnetism for **7**. Table of intermolecular interactions. CCDC numbers 883899–883904, 945424 and 945423. For ESI and crystallographic data in CIF or other electronic format see DOI: 10.1039/c3dt51839f

materials, particularly of Fe^{II}, display thermal hysteresis, and this history-dependence of their magnetic state renders them important in the development of a new generation of advanced materials for applications in data storage, display devices, and molecular electronics.[2]

Many studies have been reported into mainly monomeric SCO Fe^{II} materials in attempts to understand the fundamental interactions responsible for the strong cooperativity[3] between SCO centres in hysteretic compounds, such interactions being due to ligands and counterions involved in hydrogen bonds,[4] π–π stacking,[5] NH/π and CH/π interactions[6] and covalent linkers.[7] In recent times concerted efforts have been made to combine the spin state switching found in Fe^{II}-based SCO compounds with secondary functions such as conductivity,[8] porosity,[9] and chirality[10] to produce so-called multifunctional or hybrid SCO materials.

The bidentate chelating ability of 2,2′-dipyridylamine (dpa) in Fe^{II} complexes has led to their use in simple monomeric systems,[11] coordination polymers[12] and oxo-based Fe^{II}

polynuclear complexes.[13] However, dinuclear Fe^{II} complexes incorporating dpa-based ligands can show: (a) ferromagnetic coupling between the two HS Fe^{II} ions in, for example, $[Fe^{II}_2(dpyatriz)_2Cl_2](CF_3SO_3)_2$ (where dpyatriz = 2,4,6-tris(dipyridin-2-ylamino)-1,3,5-triazine) when the triazine ring is also involved in coordination;[14] (b) gradual, incomplete SCO transitions centred around 265 K in $[Fe^{II}_2(dpyatriz)_2(H_2O)_2(CH_3CN)_2]$-$(ClO_4)_4$,[14] and; (c) a full two step SCO transition in the complex $[Fe_2(ddpp)_2(NCS)_4]\cdot4CH_2Cl_2$, (where ddpp = 2,5-di(2′,2″-dipyridylamino)pyridine)) the latter study revealing the first structural details at the HS-LS plateau temperature.[15] 1-D Fe^{II} chains of dpa-based ligands show features such as solvent-dependent SCO behaviour,[16,17] alternating and crystallographically distinct HS and LS Fe^{II} centres along the chains[17] and SCO behaviour dependent on the degree of π–π interactions.[17,18]

From the perspective of using crown-appended ligands in SCO studies, early work by Maeda *et al.* on the series $[Fe^{III}M$-(salten)(L)] (where M = Li^+, Na^+, K^+, Rb^+, salten = 4-aza-hepta-methylene-1,7-bis(salicylideneiminate, L = *N*-(4-picolyl)-aza-15-crown-ether) showed that encapsulation of alkali metal ions in the aza-crown ether results in guest-dependent magnetic properties,[19] crystal structures were unfortunately not presented on any example. We have recently developed dipyridylamino-substituted *s*-triazine polytopic ligands containing one or two mono-aza-15-crown-5 units in an attempt to investigate any host-dependent spin-crossover properties induced by cation binding, and this resulted in formation of a polymeric heterometallic (Fe^{II}–Na^+) SCO compound which underwent a gradual, one step transition with a $T_{1/2}$ value of ∼240 K.[20] Our recent studies on a flexible, pyridyl-based linker ligand, *N*,*N*′-bis(4-pyridyl-methyl)diaza-18-crown-6 (bpmdc)[21] showed that changing the guest in, or near, the crown-ether portion of the bpmdc ligand resulted in different supramolecular packing arrangements of the well-known $[Fe^{II}(3\text{-bpp})_2]^{2+}$ SCO cation, with abrupt spin transitions being observed at higher $T_{1/2}$ values than those in conventional $[Fe^{II}(3\text{-bpp})_2]X_2$ salts.[22] The initial aim of that work was to bridge two $Fe^{II}(3\text{-bpp})(NCX)_2$ moieties with the 2-connecting bpmdc ligand in order to probe the hoped-for dinuclear product for any host–guest influences on the spin transition. The $[Fe^{II}(3\text{-bpp})_2]^{2+}$ SCO cation turned out to be the more stable product, and crystallised readily. With these previous studies in mind, we have made further developments in crown-appended systems and have investigated the host-dependent magnetic properties of a new series of Fe^{II} SCO compounds formed with a dipyridyl-amino-substituted *s*-triazine ligand that contains a bridging diaza-18-crown-6 moiety.

We present here the new dipyridylamino-triazine ligand L^1 (6-chloro-N^2,N^2-diethyl-N^4,N^4-di(pyridin-2-yl)-1,3,5-triazine-2,4-diamine) and the new diaza-18-crown-6-containing polytopic ligand L^2 (6,6′-(1,4,10,13-tetraoxa-7,16-diazacyclooctadecane-7,16-diyl)bis(N^2,N^2-diethyl-N^4,N^4-di(pyridin-2-yl)-1,3,5-triazine-2,4-diamine)), their structural formulae being shown in Fig. 1. Both ligands also contain non-coordinating aliphatic groups in an effort to introduce crystal packing effects *via* weak
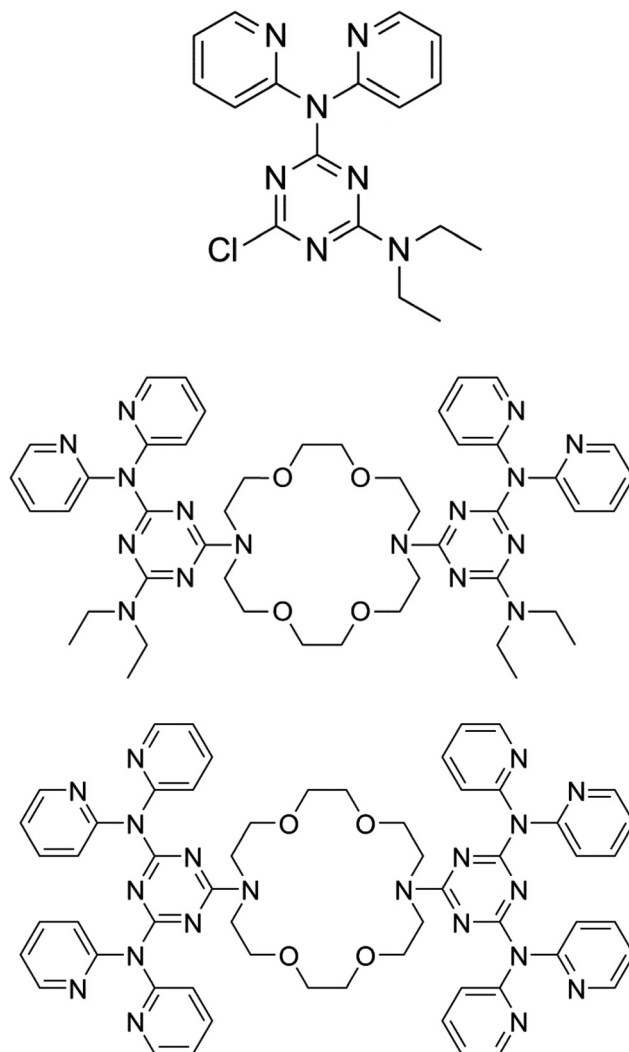

Fig. 1 Structures of ligands L^1 (top), L^2 (middle) and L^3 (bottom).

intermolecular interactions. Mononuclear Fe^{II} SCO compounds containing a related ligand, DDE, *viz.* (N^2,N^2,N^4,N^4-tetra-ethyl-N^6,N^6-di(pyridin-2-yl)-1,3,5-triazine-2,4,6-triamine) have similar aliphatic (diethyl) groups to those in L^1 and L^2 and show a crystallographic phase transition accompanied by an order–disorder transition of the diethyl groups, while undergoing a complete HS ↔ LS spin transition, with $T_{1/2}$ values above 205 K.[23] The L^2 ligand, containing a diaza-18-crown-6 moiety, was designed to produce heterometallic Fe^{II} SCO compounds where the chelating dipyridylamino groups would form an Fe^{II} SCO centre of the type $[Fe^{II}(dpa)_2(NCX)_2]$ (where NCX = NCS^-, $NCSe^-$ and $NCBH_3^-$) while having the potential for guests such as the s-block cations to be chelated within the crown ring. As in the above-mentioned crown-dipyridyl (bpmc) work, our initial aim was to make dinuclear SCO compounds in which L^2 would provide the (functional) bridge. What appeared possible 'on paper' led, however, to monomer formation, with L^2 being sufficiently flexible to allow the dpa-triazine arms to wrap around the Fe^{II} ions in an 'ear-muff' conformation. Many attempts made to insert group 1a cations

into the crown, either at pre- or post- (Fe^{II}) coordination stages, led only to monomer formation and, disappointingly, no cation binding. Thus, we present here work using the ligands L^1 and L^2, including synthesis, structures and magnetic and photomagnetic (LIESST; light-induced excited state spin trapping) behaviour on the series of complexes *trans*-[Fe^{II}(L^1)$_2$(NCX)$_2$] (X = S(**1**), Se(**2**), BH$_3$(**3**)) and *cis*-[Fe^{II}(L^2)$_2$-(NCX)$_2$]·CH$_2$Cl$_2$ (X = S(**4**), Se(**5**), BH$_3$(**6**)).

We also present a (known)[24] double-dpa-triazine 18-crown-6-linked ligand, L^3, and the first 1-D linear chain Fe^{II} derivatives thereof, *trans*-[Fe^{II}(L^3)(NCX)$_2$] (X = S, **7**; X = Se, **8**), with the formation of the crown-bridged, polynuclear species, rather than mononuclear structures of the kind found in **4–6**, possibly being due, at least in part, to the use of a markedly different synthetic methodology.

Results and discussion

Complexes **1**, **2** and **3** were isolated by the reaction of L^1 with Fe^{II}(ClO$_4$)$_2$·6H$_2$O (**1** and **2**) or Fe^{II}(BF$_4$)$_2$·6H$_2$O (**3**) and NaNCS (**1**), KNCSe (**2**) and NaNCBH$_3$ (**3**) in a 2 : 1 : 2 ratio in MeOH. For **1** and **2**, the resulting yellow solution was filtered and then diffused with Et$_2$O to produce X-ray quality yellow crystals. For **3**, the yellow solution was reduced in volume to produce a yellow precipitate, which was then dissolved in CHCl$_3$, filtered and then diffused with Et$_2$O to produce small, X-ray quality, yellow crystals. Complexes **4**, **5** and **6** were isolated by the reaction of L^2 with Fe^{II}(ClO$_4$)$_2$·6H$_2$O (**4** and **5**) or Fe^{II}(BF$_4$)$_2$·6H$_2$O (**6**) and NaNCS (**4**), KNCSe (**5**) and NaNCBH$_3$ (**6**) in a 1 : 1 : 2 ratio in MeOH. The resultant yellow precipitate was dissolved in

CH$_2$Cl$_2$, filtered and then diffused with Et$_2$O to produce X-ray quality yellow crystals. The yields for complexes **1–3** were generally quite poor, although yields for complexes **4–6** were somewhat better. Additional attempts at creating 1D chain species of the formula [Fe^{II}(L^2)(NCX)$_2$]·M$^+$ were performed, however no species of this type could be isolated.

The 1-D complexes **7** and **8** were formed in sealed tubes by reacting L^3, Fe^{II}(BF$_4$)$_2$·6H$_2$O and NaNCS–KNCSe in 1 : 1 : 2 ratio in dimethylformamide. The tubes were heated on a heat-block to 130 °C for 16 h, after which time slow cooling to ambient temperature yielded X-ray quality yellow crystals.

Single crystal structural analyses

Complexes **1–3** crystallise in the monoclinic space group $P2_1/n$, with the asymmetric unit containing half the mononuclear complexes and the unit cell containing two complete mononuclear complexes. The complexes **1–3** are structurally similar, differing only in a slight variation of bond lengths and angles (Table 1). In **1–3** each Fe^{II} is coordinated with distorted *trans* octahedral geometry (*cis* angles (N–Fe–N), 83.1(2)–96.9(2)° (**1**), 83.2(1)–96.9(1)° (**2**), 86.6(3)–93.4(3)° (**3**); *trans*, 180° (**1–3**); octahedral distortion parameter[25] Σ = 41.2° (**1**), 41.4° (**2**) and 32.6° (**3**)). Two dpa groups from two L^1 ligands chelate *via* their pyridyl nitrogens to form an equatorial plane. Completing the FeN$_6$ donor set are the two anionic cyano-based N̲CX$^-$ ligands (X = S (**1**), Se (**2**), BH$_3$ (**3**)) which bind apically, through the nitrogen, resulting in the complexes adopting the *trans* conformation (Fig. 2). Fe–N$_{NCX}$ bond distances are 2.097(4), 2.11(4) and 1.946(5) Å while average Fe–N$_{dpa}$ bond distances are 2.205, 2.22 and 1.985 Å for complexes **1**, **2** and **3** respectively.

Table 1 Selected bond lengths and angles for complexes **1–8**

| Bond(s)	**1**[a]	**2**[c]	**3**[b]	**4**[c]	**5**[c]	**6**[b]	**7**[a]	**8**[a]
Lengths (Å)								
N(1)–Fe(1)	2.097(4)	2.110(4)	1.946(5)	2.105(2)	2.101(4)	2.094(3)	1.9535(15)	1.942(2)
N(2)–Fe(1)	2.231(4)	2.227(3)	1.993(6)	2.182(2)	2.182(4)	2.134(3)	2.0107(15)	1.993(2)
N(3)–Fe(1)	2.210(4)	2.213(3)	1.981(6)	2.234(2)	2.216(4)	2.154(3)	2.0149(16)	2.011(3)
N(1′)–Fe(1)	2.097(4)	2.111(4)	1.946(5)	2.105(2)	2.101(4)	2.094(3)	1.9535(15)	1.942(2)
N(2′)–Fe(1)	2.231(4)	2.227(3)	1.993(6)	2.182(2)	2.182(4)	2.134(3)	2.0107(15)	1.993(2)
N(3′)–Fe(1)	2.210(4)	2.213(3)	1.981(6)	2.234(2)	2.216(4)	2.154(3)	2.0149(16)	2.011(3)
Angles (°)								
N(1)–Fe–N(2)	91.91(16)	91.99(13)	92.3(2)	87.83(9)	87.57(2)	86.68(11)	92.00(7)	92.12(10)
N(1)–Fe–N(3)	91.45(16)	91.44(13)	92.5(2)	91.34(9)	91.13(16)	92.57(11)	92.38(7)	92.44(10)
N(1′)–Fe–N(1)	180.00	180.0	180.00	92.47(13)	92.4(2)	89.21(16)	180.00	180.00
N(1)–Fe–N(2′)	88.09(16)	88.01(13)	87.7(2)	91.45(9)	90.77(16)	91.20(11)	88.00(7)	87.88(10)
N(1)–Fe–N(3′)	88.55(16)	88.56(13)	87.5(2)	172.71(8)	172.50(16)	174.71(11)	87.62(7)	87.56(10)
N(2)–Fe–N(3)	83.07(16)	83.08(12)	86.6(3)	82.49(7)	82.79(15)	83.94(10)	85.56(7)	86.02(10)
N(1′)–Fe–N(2)	88.09(16)	88.01(13)	87.7(2)	91.45(9)	90.77(16)	91.20(11)	88.00(7)	87.88(10)
N(2)–Fe–N(2′)	180.00	180.0	180.00	178.95(10)	177.6(2)	177.02(14)	180.00	180.00
N(3′)–Fe–N(2)	96.93(16)	96.92(12)	93.4(3)	98.29(8)	98.98(14)	98.25(10)	94.44(7)	93.98(10)
N(1′)–Fe–N(3)	88.55(16)	88.56(13)	87.50(2)	172.71(8)	172.50(16)	174.71(11)	87.62(7)	87.56(10)
N(2′)–Fe–N(3)	96.93(16)	96.92(12)	93.4(3)	98.29(8)	98.98(14)	98.25(10)	94.44(7)	93.98(10)
N(3′)–Fe–N(3)	180.00	180.00	180.00	85.56(10)	86.1(2)	86.09(14)	180.00	180.00
N(1′)–Fe–N(2′)	91.91(16)	91.99(13)	92.3(2)	87.83(9)	87.57(16)	86.68(11)	92.00(7)	92.12(10)
N(1′)–Fe–N(3′)	91.45(16)	91.44(13)	92.5(2)	91.34(9)	91.13(16)	92.57(11)	92.38(7)	92.44(10)
N(3′)–Fe–N(2′)	83.07(16)	83.08(12)	86.6(3)	82.49(7)	82.79(15)	83.94(10)	85.56(7)	86.02(10)
N(1)–C(1)–X(1)	179.30(16)	178.3(4)	176.90(7)	178.3(3)	178.3(5)	178.50(4)	179.35(18)	179.3(3)
Fe–N(1)–C(1)	173.80(16)	175.6(4)	174.80(6)	161.9(2)	160.2(4)	166.97(4)	171.93(15)	171.6(3)

[a] 100 K. [b] 123 K. [c] 173 K.
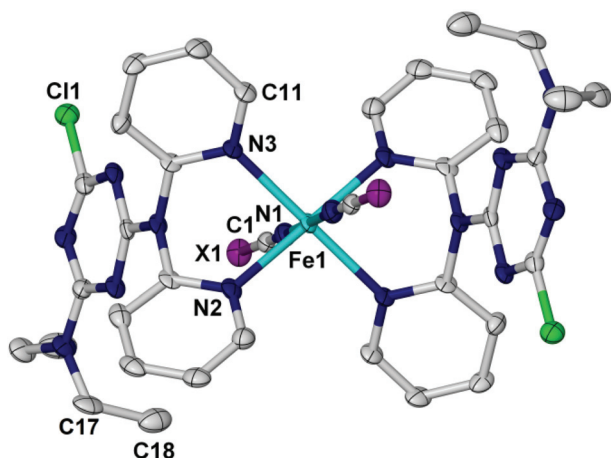
Fig. 2 Molecular structure of the L^1 family of complexes **1–3**. H atoms omitted for clarity. Nitrogen, dark blue; X (X = S (**1**), Se (**2**), BH$_3$ (**3**)), purple; chlorine, green; iron(II), turquoise.

Fig. 3 Structure of the L^2 family of complexes, **4–6**. H atoms omitted for clarity. Nitrogen, dark blue; X (X = S (**4**), Se (**5**), BH$_3$ (**6**)), purple; oxygen, red; chlorine, green; iron(II), turquoise.

1 and **2** have typical Fe–N bond lengths for high-spin (HS) Fe^{II} while the shorter Fe–N bond lengths in **3** suggest the Fe^{II} is in the low-spin (LS) state at the temperatures specified in Table 1. The diethyl 'arms' of L^1 are oriented perpendicular to the triazine ring in complexes **1–3** (Fig. 2) pointing "inwards" in **1** and **2** and "outwards" in **3** (Fig. S1†). The closest intermolecular contacts in **1** and **2** are C–H⋯Cl interactions (C18⋯Cl1, 3.415 Å (**1**), 3.401 Å (**2**)). The closest C⋯Cl distance in **3** is 3.689 Å between C17 and Cl1 (Fig. S2 and Table S1†). The closest Fe–Fe distances are 10.151 Å in **1**, 10.336 Å in **2** and 10.664 Å in **3**.

Complexes **4–6** crystallise in the orthorhombic space group *Pbcn*, with the asymmetric unit containing half the monomer and the unit cell containing four complete mononuclear complexes (Fig. 3). Complexes **4–6** are structurally similar, differing only in a slight variation of bond lengths and angles (Table 1). In **4–6** each Fe^{II} is coordinated with distorted octahedral geometry (*cis* angles, 82.49(7)–98.29(8)° (**4**), 82.79(15)–98.98(14)° (**5**), 83.94(10)–98.25(10)° (**6**); *trans* angles, 172.71(8)–178.95(10)° (**4**), 172.50(16)–177.6(2)° (**5**), 174.71(11)–177.02(14)° (**6**); octahedral distortion parameter[25] Σ = 48.43° (**4**), 47.37° (**5**) and 47.48° (**6**)). Both bidentate dpa groups from one L^2 ligand chelate *via* their pyridyl nitrogens, and the N$_6$ donor set is completed by the two anionic NCX$^-$ ligands (X = S (**4**), Se (**5**), BH$_3$ (**6**)), with complexes adopting the *cis* conformation (Fig. 3). Fe–N$_{NCX}$ bond distances are 2.102(3), 2.106(5) and 2.094(3) Å, while average Fe–N$_{dpa}$ bond distances are 2.206, 2.200 and 2.144 Å for complexes **4**, **5** and **6**, respectively. Complexes **4**, **5** and **6** have typical Fe–N bond lengths for high-spin Fe^{II} at the temperatures specified in Table 1, which for **6** lies on the spin transition. The diethyl arms from the diethylamine portion of L^2 are oriented in opposite directions, perpendicular to the triazine ring, in each of **4–6** (Fig. 3).

The flexible diaza-crown 'backbone' of L^2 ligand is substantially bent, adopting an 'ear-muff' shape and resulting in an all-*cis* conformation around Fe^{II}. This geometry exposes the
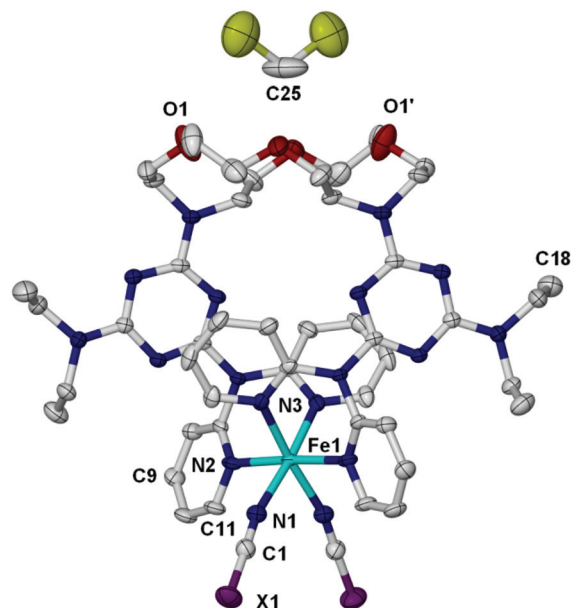
four oxygen atoms within the crown, making them available for potential hydrogen bonding to solvent molecules.

There is some residual electron density above the crown moiety in **4** and **5** which could not be modelled unambiguously, however it was determined that **6** contains a single CH$_2$Cl$_2$ molecule. The closest intermolecular contacts from this CH$_2$Cl$_2$ molecule are with the ether oxygen atoms from the crown (C25⋯O1, 3.425 Å). There are further intermolecular contacts with two dipyridylamine pyridyl groups (C9⋯Cl1, 3.690 Å) and two diethyl arms from the diethylamine portion of L^2 (C18⋯Cl1, 3.661 Å) from neighbouring molecules (Fig. S3 and Table S1†). While the residual electron density above the crown moiety in **4** and **5** suggests a number of possible solvent combinations, the microanalytical data strongly suggests it is one CH$_2$Cl$_2$ molecule, as in **6**. Numerous unsuccessful attempts were made to bind alkali-metal cations to the free diazacrown in these Fe^{II} complexes. However, the structure shown in Fig. 3 indicates that such binding is unlikely to occur due to the distorted nature of the crown upon Fe^{II} binding. To date, no cation binding has been achieved in crystals of the *cis*-[Fe^{II}(L^2)(NCX)$_2$] system. The closest Fe–Fe distances are 11.129 Å in **4**, 11.267 Å in **5** and 11.128 Å in **6**.

Complexes **7** and **8** are isostructural and crystallise in the triclinic space group $P\bar{1}$. The metal atom lies on an inversion centre and the asymmetric unit contains a section of the 1-D chain encompassing one half of the L^3 ligand bound to the Fe^{II} centre and one NCX (Fig. 5). Similarly to complexes **1** to **6**, Fe^{II} in **7** and **8** is coordinated with distorted octahedral geometry (**7**: *trans* angles equal to 180.00°; and *cis* angles ranging between 85.56(7)–94.44(7); **8**: *trans* angles equal to 180.00°; and *cis* angles ranging between 86.02(10)–93.98(10)), the former yielding an octahedral distortion parameter of Σ =
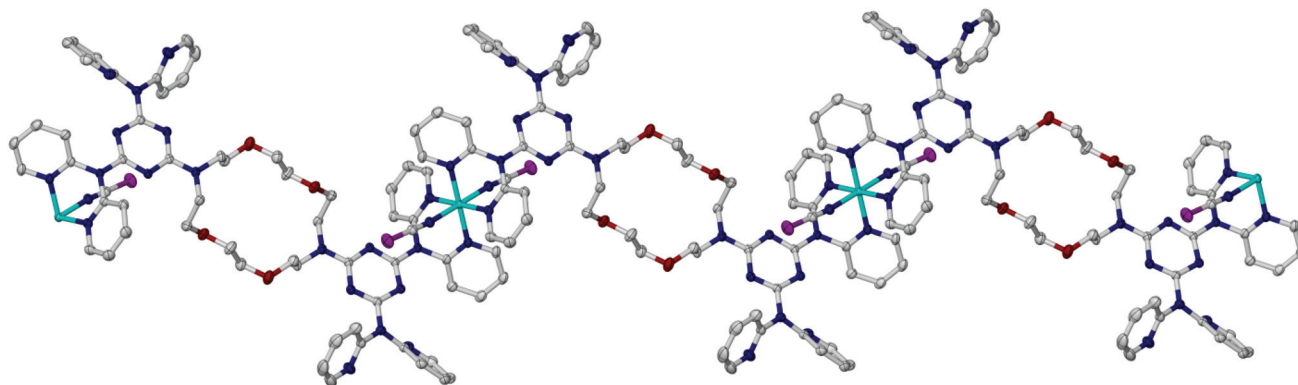
Fig. 4 Molecular structure of the L[3] pair of complexes **7** and **8**. H atoms omitted for clarity. Nitrogen, dark blue; X (X = S (**7**), Se (**8**)), purple; oxygen, red; chlorine, green; iron(II), turquoise.
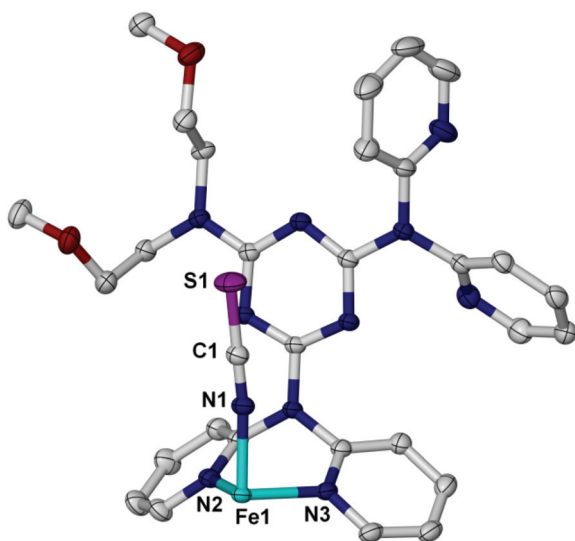

Fig. 5 Asymmetric unit of complex **7** (isostructural to complex **8**). H atoms omitted for clarity. Nitrogen, dark blue; sulphur purple; oxygen, red; chlorine, green; iron(II), turquoise.

35.28° (**7**) and 34.16° (**8**). The L[3] ligands bridge Fe[II] centres to give 1-D chains, with one dpa group from either end of each ligand coordinating to adjacent Fe[II] atoms. Two *trans* NCX ligands complete the N$_6$ coordination sphere (Fig. 4). The Fe–N$_{NCX}$ bond distances are 1.9535(15) Å (**7**, X = S); 1.942(2) (**8**, X = Se) Å, while average Fe–N$_{dpa}$ bond distances are 2.013 Å (**7**); 2.002 Å (**8**), respectively, which suggests that the spin states of the complexes are between high-spin (HS) and low-spin (LS) at 100 K. The two remaining and uncoordinated dpa groups on each L[3] ligand do not participate in any inter- or intra-molecular interactions. The closest Fe⋯Fe intra-chain and inter-chain distances are 18.770(7) and 10.486(2) Å (**7**) and 18.790(7) and 10.620(2) Å (**8**). The 1-D chains adopt a stepwise/zig-zag shape around the ligand moiety and pack together as shown in Fig. S4 and S5.† There are no solvent molecules present in the lattice in either complex.

The conformation of the 18-crown-6 ring in **7** and **8**, together with the Fe⋯Fe intra-chain separation, is reminiscent

of the complex [Co[II](NCS)$_2$(bpmdc)(H$_2$O)$_2$] in which 1-D chains are formed by the two-connecting ligand *N,N′*-bis(4-pyridyl-methyl)diaza-18-crown-6 (bpmdc), as discussed by Batten *et al.*[21] In that case the crown ring had a *trans*-pyridyl conformation with water molecules hydrogen bonded to each side of the ring.

Magnetic susceptibility studies

DC magnetic susceptibility measurements were performed on polycrystalline samples of **1**, **2**, **4–8** (Fig. 6–8), on an aged, dry, powdered sample of **3** (Fig. 6) and a freshly prepared powder sample of **3** (Fig. 7) in the 4–300 K temperature range under an applied field of 0.5 T. Since complex **3** yielded only a few crystals suitable for X-ray diffraction, a bulk powder sample was used for the magnetic measurements.

For complex **1** the $\chi_M T$ value of 3.49 cm^3 K mol^{-1} at 270 K remains essentially constant down to 130 K then decreases to 3.04 cm^3 K mol^{-1} at 70 K, remaining at this value until ~10 K, before a more rapid decrease to 2.55 cm^3 K mol^{-1} at 2 K. Thus, Fe[II] remains high-spin in character throughout the temperature range measured, in line with the Fe–N distances, the rapid decrease in $\chi_M T$ noted below 10 K being due to zero-field and Zeeman splitting effects. Complex **2** behaves similarly. The origin of the broad inflection at ~70 K is unclear, occurring also in **4**, and might indicate some small degree of spin crossover.

In contrast to the magnetism of **1** and **2**, the NCBH$_3$ compound **3** undergoes a very abrupt spin transition, beginning with a HS plateau and $\chi_M T$ value of 3.8 cm^3 mol^{-1} K at 280 K, and followed by an abrupt reduction to a $\chi_M T$ of around 0.9 cm^3 K mol^{-1}, characteristic of a mainly LS state, upon cooling to 170 K. This spin transition has a $T_{1/2}$ = 210 K and shows little or no hysteresis (Fig. 6).

To further investigate the magnetic behaviour of **3**, susceptibility measurements were performed for this complex on a freshly prepared and powdered sample, as seen in Fig. 7. This sample was a hydrate, as determined by microanalysis and TGA data (see Experimental section) and displayed an abrupt SCO with hysteretic behaviour. The plateau value of 3.2 cm^3
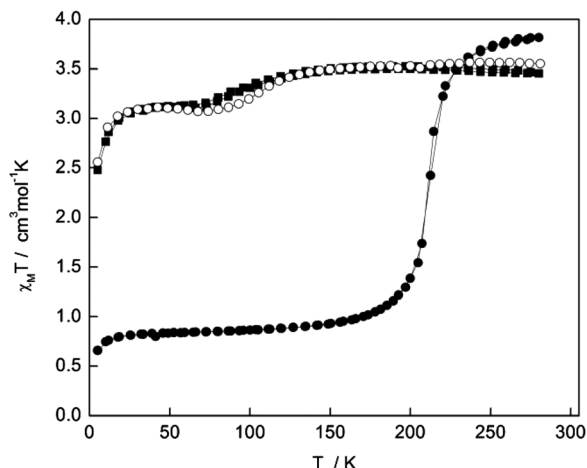
Fig. 6 Plot of $\chi_M T$ vs. T for **1** (○), **2** (■) and **3** (●) (aged, dry powder) between 2–300 K in an applied field of 0.5 T.
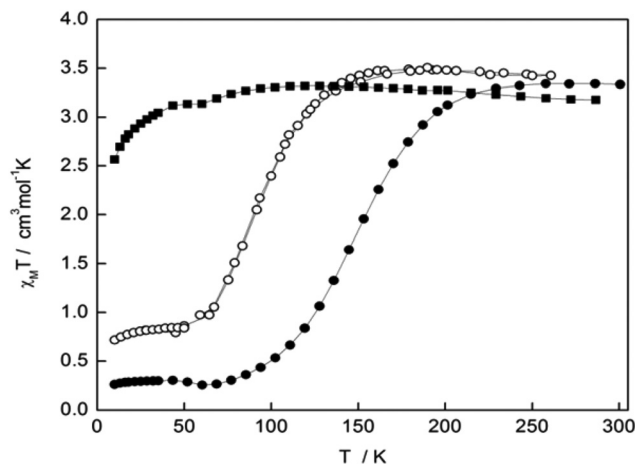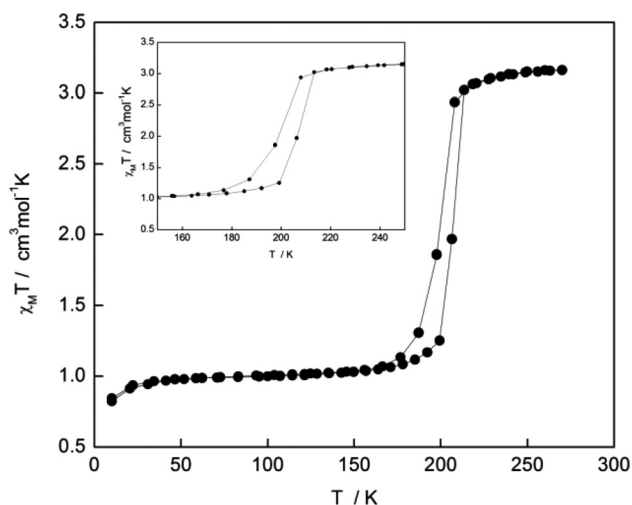

Fig. 7 Plot of $\chi_M T$ vs. T for **3**·1.5H$_2$O (●) (freshly prepared powder) between 5–300 K in an applied field of 0.5 T.

mol^{-1} K observed for the HS state, at room temperature, decreases abruptly to 1.0 cm^3 mol^{-1} K at 170 K ($T_{1/2} \approx 203$ K). While in the heating mode, $T_{1/2}$ is shifted to a higher temperature of ~210 K; thus ΔT is ≈7 K. PXRD studies of these powder samples of **3** revealed them to be largely amorphous and, thus, definitive comparison to the calculated diffractogram was not possible, although we are confident the structure is similar to that of the crystallographic sample.

To further investigate the thermal hysteresis (width of 7 K) found in the magnetic susceptibility measurements of **3**·1.5H$_2$O (Fig. 7) a differential scanning calorimetry (DSC) measurement was undertaken on the same sample between 123 K and 273 K with a heating and cooling rate of 5 K min^{-1} and the experimental curve between 170 K and 240 K is shown in Fig. S6 (ESI†). An exothermic peak was observed at 203.2 K during the cooling cycle and upon heating an endothermic peak at 209.6 K is observed. The endothermic peak is shifted from the exothermic peak by 6.4 K indicating a small thermal

Fig. 8 Plot of $\chi_M T$ vs. T for **4** (■), **5** (○) and **6** (●) between 5–300 K in an applied field of 0.5 T.

hysteresis. This is in good agreement to the thermal hysteresis observed in the magnetic susceptibility measurements (Fig. 7) given that the scanning rates in the MPMS settle mode (6.7 K min^{-1}) are a little faster than the DSC measurement scan rates (5 K min^{-1}). The enthalpy changes, ΔH, associated with the spin transition have been calculated independently for the heating and cooling cycles and the average values reported. This results in an average ΔH value of 2.7 kJ mol^{-1} while the corresponding average change in entropy value, ΔS, is calculated to be 13.1 J mol^{-1} K^{-1} (using the relation $\Delta H = T\Delta S$ ($T = (T_{exo} + T_{endo})/2 = 206.4$ K)). The thermal behaviour was consistent through repeated heating and cooling cycles and the ΔH and ΔS values are within the range of that expected for Fe^{II} spin transitions.

For complex **4** the $\chi_M T$ value of 3.18 cm^3 K mol^{-1} at 287 K increases slightly to reach a value of 3.32 cm^3 K mol^{-1} at 119 K and then decreases down to a final $\chi_M T$ value of 2.57 cm^3 K mol^{-1} at 10 K suggesting the Fe^{II} remains high-spin in character throughout the temperature range measured. Compound **5** is shown to undergo a gradual spin transition, when measured between the temperature range 261–10 K, with $T_{1/2}$ occurring at ~100 K as evidenced by the gradual decrease of the room temperature $\chi_M T$ value of 3.3 cm^3 K mol^{-1} to a final value of 0.7 cm^3 K mol^{-1} at 10 K. Hysteretic behaviour was not observed in the heating and cooling modes. For complex **6** the $\chi_M T$ value of 3.34 cm^3 K mol^{-1} at 300 K remains constant until around 220 K, whereupon a gradual spin transition occurs leading to a final $\chi_M T$ value of 0.26 cm^3 K mol^{-1} at 10 K. The $T_{1/2}$ value is around 150 K with no evidence of hysteretic behaviour. Complex **7** showed a gradual spin transition, with $T_{1/2} \sim$ 130 K (Fig. S12; ESI†). Although we could obtain a suitable single crystal of complex **8** for crystallographic studies we were unable to obtain enough pure crystalline product for magnetic susceptibility measurements.

Cooperativity and anticooperativity in 3, 5 and 6

As indicated above, the polycrystalline mononuclear spin crossover complexes **3**, **5** and **6** generally display no hysteresis,

although the freshly prepared powder sample of $3 \cdot 1.5H_2O$ shows an abrupt, single step hysteretic crossover with a difference of 7 K between $T_{1/2\uparrow}$ and $T_{1/2\downarrow}$. The aged powder of **3** shows the same sharp transition, at the same $T_{1/2}$, but with no hysteresis. Thus, prior to fitting the γ_{HS} data (see below) we anticipated that complex **3** showed stronger cooperativity than the others. At a qualitative level, the intermolecular interactions summarised in the Introduction that commonly contribute to cooperativity,[5f] *viz.*, van der Waals, hydrogen bonding,[4e] π–π stacking, might be expected to reveal some such effects that are present and dominant in **3** but not in **5** and **6**, even though **3** has different ligand milieu compared to **5** and **6**. In complex **3** there is an intermolecular contact C–H⋯Cl from a diethyl arm of L^1 to the triazine bound chlorine of a neighbouring complex (C17⋯Cl1, 3.689 Å) (Fig. 2 and S2, Table S1†). It is possible the solvated species $3 \cdot 1.5H_2O$ does display stronger interactions compared to **3**. Complex **6** shows intermolecular contacts from the CH_2Cl_2 solvate with the ether oxygens from the crown (C25⋯O1′, 3.425 Å) and there are further intermolecular contacts from the CH_2Cl_2 solvate with two dipyridylamine pyridyl groups (C9⋯Cl1, 3.690 Å) and with two diethyl arms from the diethylamine portion of L^2 (C18⋯Cl1, 3.661 Å) from neighbouring molecules (Fig. S3 and Table S1†). Although we cannot unambiguously model the residual electron density above the crown in **5** as a dichloromethane molecule, the microanalytical data on the bulk sample suggests a single dichloromethane solvate as in **6** and as such we would expect similar intermolecular interactions to complex **6**, described above.

However, it is difficult to make definitive conclusions in regard to differences in cooperativity from the above discussion of weak crystallographic interactions. More quantitative analyses of cooperativity[26–28] have involved calculations of the Slichter and Drickamer thermodynamic (mean-field) type (eqn (1)),[29] to simulate spin transition γ_{HS} (fraction of high-spin) data

$$\ln[(1-\gamma_{HS})/\gamma_{HS}] = (\Delta H_{HS\leftrightarrow LS} + \Gamma(1-2\gamma_{HS}))/RT - \Delta S_{HS\leftrightarrow LS}/R \tag{1}$$

and deduce interaction parameters, Γ (or cooperativity factors $C = \Gamma/2RT_{1/2}$). Tchougréeff *et al.*[30] have recently discussed the sign of Γ, with a positive sign being indicative of cooperative interactions and a negative sign being indicative of anticooperative interactions. This group used atom–atom potential calculations to underpin the Γ values. It contrasts with the work of Robert *et al.*[31] who have calculated electrostatic Madelung fields acting on the Fe and N centres, by use of *ab initio* CASSCF methods to deduce the cooperativity parameter Γ_{pol} (eqn (2)) where:

$$\Gamma_{pol} = \Delta Q(\delta V_{HS} - \delta V_{LS}) \tag{2}$$

Here δV_{HS} and δV_{LS} stand for the differences in potential upon the Fe and N atoms, and ΔQ is the difference in atomic charges. This approach was applied to families of *cis*- and

trans-[Fe(L)$_2$(NCS)$_2$] monomers.[31] We briefly explore this method for complex **3**, below.

Turning again to the Slichter and Drickamer approach, we have obtained good and reliable fits to eqn (1) for complexes **3**, **5** and **6** when using the following parameter sets:

3: $\Delta H = 18.8$ kJ; $\Delta S = 89.4$ J K^{-1} mol^{-1}; $\Gamma = 2.75$ kJ mol^{-1} ($T_{1/2} = 200$ K, $C = 0.83$)

5: $\Delta H = 11.7$ kJ; $\Delta S = 121$ J K^{-1} mol^{-1}; $\Gamma = -1.85$ kJ mol^{-1} ($T_{1/2} = 100$ K, $C = -1.11$)

6: $\Delta H = 24.0$ kJ; $\Delta S = 162$ J K^{-1} mol^{-1}; $\Gamma = -5.05$ kJ mol^{-1} ($T_{1/2} = 150$ K, $C = -2.02$)

The plots for best fit are shown in Fig. 9, for **5** and Fig. S7 and S8 (ESI†) for **3** and **6**. Use of positive Γ values for **5** and **6** gave very poor fits and thus we are confident that, within the limitations of the mean field model, the crown complexes **5** and **6** display anticooperative interactions whilst complex **3** is cooperative. While these fits were for the non-hysteretic sample of **3** and the experimental DSC values were for the hysteretic sample $3 \cdot 1.5H_2O$, the ΔH and ΔS values from DSC are some six times smaller. Other groups have noted such discrepancies but not to the same degree.[32]

In general, the values of ΔH, ΔS and Γ (and C), above, are typical for Fe^{II}L$_2$(NCX)$_2$ spin-crossover materials, with Γ for **6** larger in size than reported values.[30,33,34] However, there are few, if any, systems with negative Γ values reported to make comparisons to **5** and **6** for both of which the shapes and slopes of the $\chi_M T$ (or γ_{HS}) curves are 'gradual', albeit with different $T_{1/2}$ temperatures. When Γ is positive, larger Γ (or C) values result in more abrupt curves,[33] but we don't have enough data to make such correlations when Γ is negative. In comparing outcomes for **5** and **6**, it may be noted that the ΔH and ΔS values are bigger in the X = NCBH$_3$ case **6**; such increases in best-fit ΔH values when changing NCSe for NCBH$_3$ have also been noted in other crossover siblings.[33,34]
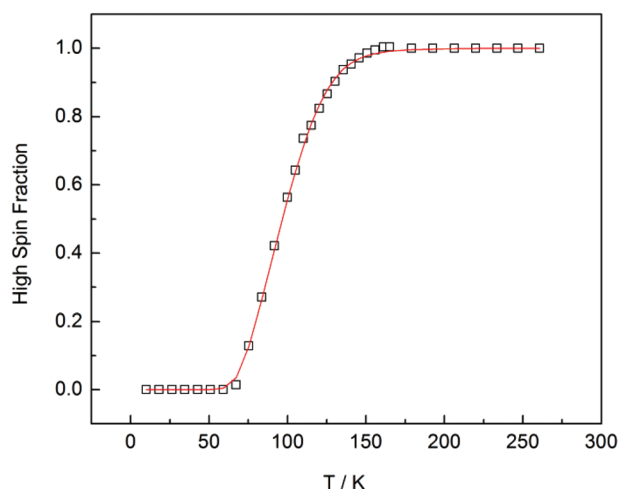

Fig. 9 Plot of high-spin fraction, *vs.* temperature, for complex **5** with the red line being the best fit to the Slichter–Drickamer mean-field model (eqn (1) in script) and the ΔH and ΔS and Γ values given in the script. The LS χ_M(TIP; 2nd order Zeeman) contribution (see Fig. 8) has not been included.

Theoretical studies on 3

To further understand the cooperativity, we have performed DFT calculations on complex **3** to compute the Γ and the C parameters and also to gain insight into the electronic structure of the HS molecule. For calculations we have employed B3LYP-D2 including dispersion effects of Grimme,[35] as weak interactions need to be accounted for. All calculations employ the Ahlrich TZV basis set for all the atoms[36] and have been performed using the Gaussian 09 suite of programs.[37] We have analyzed the HS wavefunction of the complex **3** and the computed spin density plot is shown in Fig. 10. The spin density on the Fe atom is estimated to be 3.81 revealing a moderate delocalization of spin densities to other atoms, particularly to the coordinating N atoms. Within the two sets of nitrogen atoms in the coordination sphere (Npy and N of NCBH$_3$), the distinction is visible with nitrogen of the NCBH$_3$ group having a spin density of 0.03 while the Npy atoms have close to 0.05. A smaller spin density on the N atom of NCBH$_3$ group is due to the presence of the BH$_3$ group (weak σ donating ability) and these electronic differences observed suggest that the axial ligation can significantly influence the observed magnetic properties as evident in the complexes **1–3** studied. While only a negligible amount of spin density is detected at the BH$_3$ group, other pyridine-type nitrogen atoms propagate spin densities *via* spin polarisation (see green shades in Fig. 10). However, as the ligands are large the propagation does not reach toward the end of the molecular chain, revealing that electronic factors such as spin polarization are unlikely to be important in determining the SCO properties. Thus, the expected cooperativity is purely electrostatic in nature. The computed Mulliken charges reiterate this statement as the charge computed on Fe is 0.98 for HS and 0.70 for the LS state while the B atom of the BH$_3$ group bears a significant negative charge both in the HS and LS state (∼−0.34).

To further probe the cooperativity effects, we have employed the protocol of Robert *et al.*[31] and have attempted to compute the C parameter. This group[31] computed the cooperativity using CASSCF methodology. In their report, they found that the Γ parameter has two contributions, Γ_{vdw}, accounting for all the weak interactions between the molecules, and Γ_{pol}, accounting for the charge redistribution due to ligands, geometry reorganization for different spins and lattice expansion within the system. Here the Γ_{vdw} is estimated as the energy difference between the like spin and unlike spin in the crystal lattice, *i.e.* $\Gamma_{vdw} = (2E_{LS,HS} - E_{LS,LS} - E_{HS,HS})$. For complex **3** this is estimated to be 70 K and this value is much smaller than the value reported for other complexes.[31] As this value is related to intermolecular interactions, and as the crystal structure suggests that the complex **3** does not have any significant intermolecular interactions, a small computed Γ_{vdw} is consistent with this expectation. When taking into consideration only Γ_{vdw}, the C parameter is estimated to be 0.21. Although the sign is reproduced compared to the experiment, the magnitude is underestimated. Assuming Γ_{vdw} = 70 K, one can estimate $\Gamma_{pol} \sim 260$ K from the experimental measurement. This is in line with the fact that the Γ_{pol} has been termed as the prominent factor controlling the C value.[31] Unfortunately, since the crystal structure of the HS form is unavailable, Γ_{pol} cannot be directly computed from eqn (2), above. Using the approximation that the LS lattice structure also applies to the HS form, we get an overestimation of the C to be 5.2, which is perhaps not surprising.

Reflectivity and photomagnetic studies on the crown-ligand (L^2) – iron(II) SCO complexes 5 and 6

Optical reflectivity and photomagnetic LIESST (light induced excited spin state trapping) studies were carried out on compounds **5** and **6**. The spin crossover can be monitored by following the thermal behaviour of the visible spectrum measured by diffuse reflectance. The results for **5** and **6** were similar, so the data for **6** are focussed upon here.

For both complexes, the absorption spectra at 280 K are mainly made up of a large band around 850 nm that can be attributed to the d–d transition of Fe^{II} in its HS state. Upon cooling, an intense band grows around 600 nm that reflects the MLCT occurring in the LS state and indicates that the HS to LS spin crossover occurs between 280 K to 80 K (Fig. 11 and S9†). For **5**, the small variation of the 850 nm band indicates that some HS residue could be present at low temperature. In the case of **6**, an almost isosbestic point is observed at 740 nm, indicating the occurrence of an equilibrium. In addition, the band at 850 nm almost disappears at 80 K, indicating that the spin-crossover is complete. From the reflectivity data recorded at 600 nm (Fig. 11 and S9†), the spin crossover temperatures can be estimated at 130 K for **5** (Fig. S9†) and 170 K for **6** (Fig. 11). Moreover, in **6**, the evolution of the reflectivity signals at 550 nm and 850 nm are inversed in agreement with the equilibrium observed in the absorption spectra.

Below 80 K, the 600 nm band decreases while the 850 nm band increases (in **6** especially) as we decrease temperature. This indicates the occurrence of photo-induced colour change and therefore the LIESST effect at the surface of the sample. This is particularly visible on the reflectivity measurements at 600 nm (**5**) and 550 nm (**6**), where the signal increases,
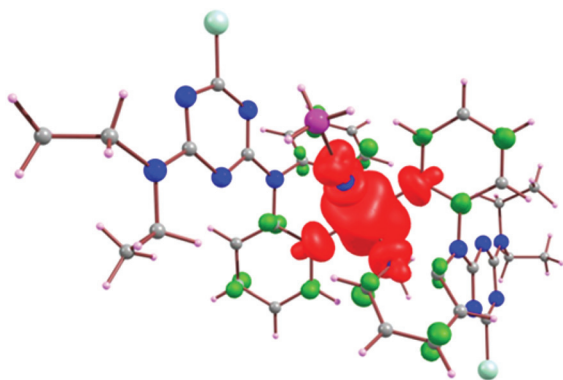

Fig. 10 B3LYP-D2 computed spin density plot for complex **3**. Here red and green shade represent positive and negative spin densities.
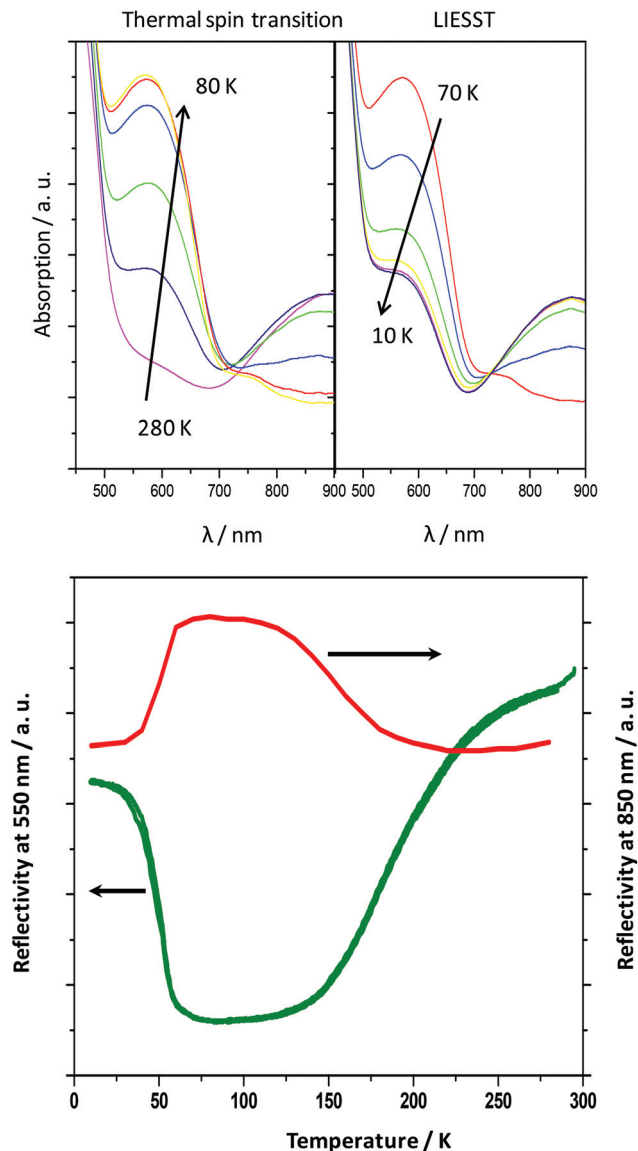
Thermal spin transition / LIESST

Fig. 11 Thermal dependency of the absorption spectra under light irradiation (top) and intensity of the reflectivity signal at 550 (green) and 850 nm (red) (bottom) for *cis*-[Fe^{II}(L^2)(NCBH$_3$)$_2$], **6**.

indicating the population of the HS state. In **6**, the decrease of the 850 nm signal also indicates the occurrence of HS population below 80 K.

For the photomagnetic studies on **5** and **6**, irradiation was performed at different wavelengths and the best one was found to be at in the green band (514 nm) with a power of 5 mW cm^{-2}. Only the LIESST effect was observed and no reverse-LIESST. When the photostationary limit was reached, the T(LIESST) curve was recorded (Fig. 12 and S10†). The increase of $\chi_M T$ from 10 to 40 K observed for **5** usually follows from the Fe^{II} zero-field splitting. This increase is not observed in **6**, probably due to efficient relaxation of the photo-induced HS state. The maximum $\chi_M T$ value gives some information on the photoconversion efficiency, this being around 90% for **5** and 66% for **6**. Above 40 K, the $\chi_M T$ product decreases and the
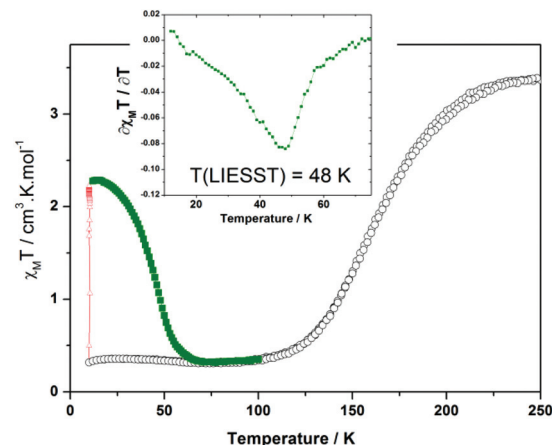

Fig. 12 Thermal behaviour of the $\chi_M T$ product of **6** before irradiation (O), during irradiation (△) and in the dark after irradiation (■). The insert presents the derivative of the thermal $\chi_M T$ as a function of T (in the dark after irradiation); the minimum allows the determination of the T(LIESST) value.

baseline is recovered. The minimum value of the derivative $\partial \chi_M T/\partial T$ gives the value of the T(LIESST) temperature estimated at 55 K for **5** and 48 K for **6**.[38]

Several kinetic runs were recorded to characterise the relaxation process (Fig. 13 and S11†). For both **5** and **6**, the relaxation curves follow an exponential shape. To extract the relaxation rate constant at each temperature, we employed a stretched exponential law, with a distribution σ of the activation energy E_a. Fig. 13 and S10† show the fit of the kinetics. The thermodynamic parameters E_a, k_∞ and σ were extracted from the Arrhenius plot (ln k_{HL} vs. $1/T$) and the best-fit parameters for **5** are: E_a = 540 cm^{-1}, k_∞ = 1500 s^{-1}, σ = 33 cm^{-1}; and for **6**, are: E_a = 196.4 cm^{-1}, k_∞ = 0.659 s^{-1}, σ = 49.7 cm^{-1}. These low activation energies are probably indicative of little communication occurring in the lattices of **5** and **6**, in broad agreement with the anticooperativity discussion above.
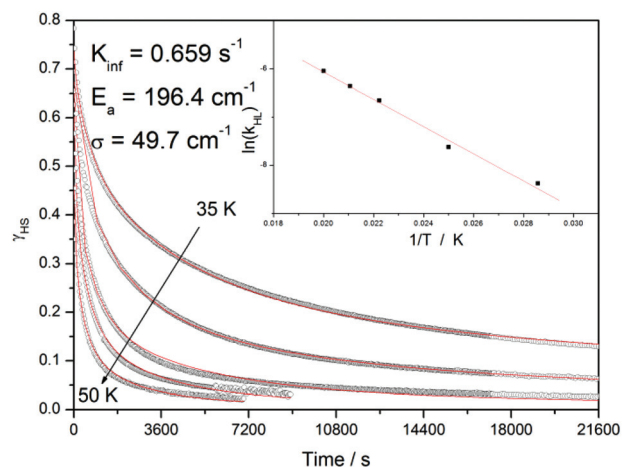

Fig. 13 Plot of the different relaxation kinetics recorded as a function of the temperature (35, 40, 45, 47.5 and 50 K) for **6**. The red lines are calculated using the parameters given in the text. The inset is the fit to the Arrhenius equation.

Discussion

Complexes **1–3** form a series of type *trans*-[Fe^{II}(L^1)$_2$(NCX)$_2$], where they differ only in NCX$^-$ substituent. While the X = S and Se derivatives remain mainly high-spin, the stronger field X = BH$_3$ complex shows spin-crossover. The $T_{1/2}$ values in the L^2 complexes *cis*-[Fe^{II}(L^2)(NCX)$_2$]·CH$_2$Cl$_2$, **4–6**, likewise follow the expected changes for the ligand-field strengths NCS < NCSe < NCBH$_3$. Only the powder sample of **3**·1.5H$_2$O showed thermal hysteresis. In attempting to rationalise the hysteresis and associated cooperativity in **3**, we note that the most significant feature of **3**, at least when considering the crystal structure, is the presence of a single C–H···Cl contact (*vide infra*). For a weakly hysteretic sample we would expect a degree of cooperativity mediated by such interactions. We can postulate that the water of hydration molecule suggested by microanalysis and TGA in the freshly prepared powder sample of **3** may introduce some additional H-bonding intermolecular contacts, structural information not available to us from our single crystal structure determination. Using the Slichter and Drickamer model,[29] fits to the $\chi_M T$ *vs.* *T* data for **3** confirm the co-operative nature resulting in a positive cooperativity factor *C* as seen for similarly abrupt spin transitions.[30,33,34]

The anticipated chain structure of complexes containing L^2, with the dpa chelating groups binding to separate Fe^{II} centres, and the NCX$^-$ ligands being *trans* to each other, did not form. The 'ear-muff' conformation of L^2 appears, from the data thus far obtained, to be a very stable form that favours formation of mononuclear SCO products. Incorporation of an alkali-metal or alkaline earth metal cation into the crown prior to forming the Fe^{II} compound would be expected to 'flatten' the crown ring and assist polymer formation, but we have not been able to achieve cation binding to the L^2 ligand to date. Finally the dichloromethane solvate molecule present in **6** (and assumed to be present in **4** and **5** based on microanalytical data) is involved in several C–H···O and C–H···Cl intermolecular interactions (Fig. S3 and Table S1†) which may play a part in the gradual spin transitions in **5** and **6**. In contrast to **3**, use of the Slichter and Drickamer model[29] to fit the $\chi_M T$ *vs.* *T* data for **5** and **6** resulted in negative cooperativity factors (*C*) suggesting the observed gradual spin transitions are anticooperative in nature. Guionneau *et al.*[39] reported an inverse correlation between $T_{1/2}$ and the change in the geometric distortion parameter $\Delta\Theta$ for low-spin and high-spin states in a range of complexes of type *cis*-[Fe^{II}(NCS)$_2$(L)$_2$], where L is a bidentate N-donor chelate.[5f] Unfortunately we have no structural details of **5** and **6**, which are of the [Fe^{II}(NCS)$_2$(L)$_2$] type, in the low-spin state and so cannot make a direct comparison to this correlation.

1-D chain structures were formed by ligand L^3, wherein only one of the dpa moieties on each end of the crown linker binds to Fe^{II}, and the remaining dpa moieties remain uncoordinated between neighbouring 1-D chains (Fig. S4†). These uncoordinated dpa moieties are not involved in π–π stacking with equivalent groups on neighbouring chains, despite appearances in Fig. S4.† It remains unclear why L^2

forms discrete monomers (**4–6**) while L^3 forms extended 1-D chains (**7** and **8**). The structural differences of L^2 and L^3 can be seen in Fig. 1, where the diethylamine arms found in L^2 are replaced by dpa groups in L^3. On inspection of complexes **4–6** (Fig. 3) there seems little reason on steric grounds for complexes involving L^3 not to form discrete monomers, as in **4–6**, where the additional dpa group could remain uncoordinated. The synthesis of **7** and **8** to form the 1-D chains, however, is markedly different to that of **4–6** (see Experimental section). The synthesis of **4–6** was undertaken at ambient temperature in methanol, whereas **7** and **8** are formed by heating in DMF at 130 °C for 16 hours in a sealed vial and cooling to get crystalline product. It is reasonable to suggest that the higher reaction temperatures in the synthesis of **7** and **8** may play a large role in the formation of 1-D chains instead of discrete monomers as is the case in **4–6**. There are other examples of temperature affecting the crystalline product, for example in polynuclear MOF products made by hydrothermal methods.[40]

Regarding the photomagnetic studies, compounds **5** and **6** are sensitive to the LIESST effect and T(LIESST) values were measured giving values of 55 K for **5** and 48 K for **6** which belong to the $T_0 = 100$ K line in the graph of T(LIESST) *vs.* $T_{1/2}$,[38] where T(LIESST) $= T_0 - 0.3T_{1/2}$. From databases on many mononuclear FeN$_6$ coordination environments, this line is indicative of FeN$_4$(NCX)$_2$ coordination spheres, as expected.[38] Moreover, with stronger NCX ligand fields we would expect higher $T_{1/2}$ and lower T(LIESST) values. Compounds **5** and **6** clearly follow this trend. Despite the large crown moiety in these complexes, no particular constraints seem to be imposed to the coordination sphere. This is linked to the small octahedral distortion parameter $\Sigma = 47.37°$ (**5**) and $47.48°$ (**6**) in the HS state. This parameter has been shown to be important in the improvement of the photo-induced HS state lifetime. Such weak Σ agree with the relatively small T(LIESST) values.

Conclusion

Six new Fe^{II} mononuclear complexes and two 1-D chain complexes of dpa-triazine ligands have been synthesised and fully characterised, three of them showing spin crossover. The mononuclear compounds may be categorised into two different series of discrete [Fe^{II}L$_n$(NCX)$_2$] complexes, with the common variant within each series being the terminal NCX$^-$ ligands. Both series contained diethylamino substituents in the triazine ring of the ligands to see if they engendered weak intermolecular interactions that would influence cooperativity in the spin transition. No such influence could be detected. The series with a linking crown ligand situated between two dpa moieties, L^2, did not form the anticipated chain *trans* structures, but rather formed mononuclear *cis* species. 1-D chain complexes were formed, however, when using the crown-linked ligand L^3 that has two dpa units at each end, only one of which coordinates to Fe^{II}. Compounds **5** and **6**, containing

the crown-linked ligand L^2, gave well resolved photomagnetic/ LIESST behaviour and relaxation kinetics.

Further, we have attempted to shed light on cooperativity in the SCO examples by structural and more quantitative calculational approaches of the Slichter–Drickamer mean-field approach[29] (for **3, 5, 6**) and by DFT and *ab initio* methods (for **3**), with broad agreement found between the methods but without being able to pin down precise intermolecular structural reasons for the weak cooperativity noted.

Further studies in this area will examine the confluence of such cooperativity effects and the weak intermolecular contacts such as those reported here. We will also seek to investigate the role, if any, of the synthetic methods used to form monomeric/1-D chain species in related Fe^{II} dpa based SCO materials. Finally, in regard to cation binding to the crown moieties in the L^2 and L^3 compounds, no binding has been noted to date but this will be pursued further.

Experimental

Syntheses

All manipulations were performed under aerobic conditions using chemicals as received, unless otherwise stated. **Caution!** Care should be taken when using the potentially explosive perchlorate Fe^{II} salts. 4,6-Dichloro-*N*,*N*-diethyl-1,3,5-triazine-2-amine (below) was prepared using a modification to the conditions reported by Hermon *et al.*[41] Ligand L^3 was prepared using the method of Gamez *et al.*[24]

4,6-Dichloro-*N*,*N*-diethyl-1,3,5-triazine-2-amine

Cyanuric chloride (3.5 g, 18.9 mmol) and *N*,*N*-diisopropylethylamine (DIPEA) (2.9 ml, 16.6 mmol) were dissolved in 100 ml THF and the solution was stirred and cooled to −30 °C. Separately, diethylamine (0.7 g, 9.57 mmol) was dissolved in 100 ml of THF and added, dropwise, to the stirred solution of cyanuric chloride–DIPEA kept at −30 °C, over the course of four hours. After complete addition, the solution was left to reach room temperature and stirred for a further 24 h. The solution was then reduced in volume, *in vacuo*, to form a yellow solid which was dissolved in 200 ml of deionised water. This was extracted with Et_2O (2 × 50 ml) and the combined organic extracts were filtered, dried, and reduced *in vacuo* to give a yellow solid product. The yellow solid was dissolved in boiling hexane, the solution filtered, and the clear filtrate was slowly reduced under a flow of N_2 to give white crystals. Yield: 1.74 g (41.6%). MW: 221.09. MP: 78.1–78.6 °C. IR (ATR cm^{-1}): 2996 (w), 2952 (w), 2874 (w), 2114 (w), 1982 (w), 1582 (w), 1559 (s), 1471 (s), 1432 (s), 1376 (m), 1347 (s), 1325 (s), 1226 (s), 1154 (s), 1091 (m), 1038 (m), 980 (m), 904 (w), 809 (s), 791 (m), 782 (m), 594 (w). MS (ESI+) *m/z*: 221 [M + H]$^+$. ^{1}H-NMR (200 MHz, CDCl$_3$): δ 3.62 (q, 4H, *J* = 7.1 Hz), 1.22 (t, 6H, *J* = 7.1 Hz). ^{13}C-NMR (400 MHz, CDCl$_3$): δ 170.14, 164.08, 42.63, 12.71. Microanalysis: Found C 38.25, H 4.68, N 25.28%. Calculated for C$_7$H$_{10}$Cl$_2$N$_4$ C 38.03, H 4.56, N 25.34%.

6-Chloro-N^2,N^2-diethyl-N^4,N^4-di(pyridin-2-yl)-1,3,5-triazine-2,4-diamine (L^1)

4,6-Dichloro-*N*,*N*-diethyl-1,3,5-triazine-2-amine (1.29 g, 5.84 mmol) and 2,2′-dipyridyl-amine (1.0 g, 5.84 mmol) were dissolved in 30 ml of MeCN. DIPEA (2.9 ml, 16.6 mmol) was added, and the solution was stirred under reflux for three days. Following this, the solution was reduced in volume *in vacuo* to give a yellow solid. 20 ml of deionised water was added, and the product extracted with CHCl$_3$ (2 × 30 ml). The organic extracts were combined and reduced, giving a brown solid that was subsequently recrystallised from a 1 : 1 (v/v) acetone–hexane solution to produce yellow needles, isolated by filtration. Yield: 0.988 g (44.5%). MW: 355.82. MP: 161.1–161.5 °C. IR (ATR cm^{-1}): 3337 (m), 3039 (w), 2946 (w), 2807 (w), 2358 (w), 2101 (w), 1995 (w), 1658 (m), 1593 (s), 1554 (s), 1502 (s), 1449 (s), 1303 (m), 1244 (m), 1148 (m), 1095 (m), 1027 (m), 984 (m), 934 (m), 882 (m), 839 (m), 771 (sh), 671 (m). ^{1}H-NMR (400 MHz, DMSO-d_6): δ 8.35 (2H, m), 7.87 (2H, m), 7.58 (2H, m), 7.26 (2H, m); 3.51 (2H, q, *J* = 7.0 Hz), 3.23 (2H, q, *J* = 7.0 Hz), 1.09 (3H, t, *J* = 7.0 Hz), 0.92 (3H, t, *J* = 7.80 Hz). ^{13}C-NMR (500 MHz, CDCl$_3$): δ 166.07, 155.39, 149.13, 145.13, 138.33, 123.74, 122.00, 110.38, 58.07, 13.66. MS (ESI+) *m/z*: 356 [M + H]$^+$, 378 [M + Na]$^+$. Microanalysis: Found C 56.88, H 5.29, N 26.31%. Calculated for C$_{17}$H$_{18}$ClN$_7$, C 57.38, H 5.10, N 27.55%.

6,6′-(1,4,10,13-Tetraoxa-7,16-diazacyclooctadecane-7,16-diyl)bis-(N^2,N^2-diethyl-N^4,N^4-di(pyridin-2-yl)-1,3,5-triazine-2,4-diamine) (L^2)

L^1 (1.66 g, 4.67 mmol), diaza-18-crown-6 (0.6 g, 2.29 mmol) and diisopropylethylamine, DIPEA (1.2 ml, 6.87 mmol) were dissolved in 40 ml of 1 : 1 (v/v) MeCN–toluene, and refluxed over the course of four days. After this time, the solution was reduced *in vacuo* to give a brown solid, which was subsequently re-dissolved in 30 ml of deionised water and extracted with CH$_2$Cl$_2$ (2 × 30 ml). The organic extracts were combined and reduced *in vacuo* to give an off-white coloured powder. This powder was then washed with warm ethanol to yield a clean white powder. Yield: 1.81 g (87.7%). MW: 901.07. MP: 198.4–200.1 °C. ^{1}H NMR (200 MHz, d_6-DMSO): δ 8.30 (m, 4H), 7.62 (m, 4H), 7. 55 (m, 4H), 6.99 (m, 4H), 3.65–3.07 (m, 32H), 1.08 (t, 6H, *J* = 6.8 Hz), 0.91 (t, 6H, *J* = 6.8 Hz). ^{13}C NMR (500 MHz, DMSO-d_6): δ 211.90, 165.98, 156.58, 148.50, 136.86, 123.29, 120.30, 70.59, 69.81, 63.48, 58.47, 48.22, 41.46, 18.61, 13.53, 8.71. MS (ESI+) *m/z*: 901 [M + H]$^+$, 923 [M + Na]$^+$. IR (cm^{-1}): 2969 (m), 2894 (m), 2088 (w), 1588 (m), 1547 (s), 1519 (s), 1496 (s), 1474 (s), 1417 (s), 1388 (s), 1367 (m), 1292 (s), 1259 (m), 1234 (m), 1190 (w), 1165 (w), 1142 (m), 1075 (m), 995 (w), 932 (w), 879 (w), 808 (m), 774 (m). Microanalysis: Found C 60.92, H 6.85, N 24.54%. Calculated for C$_{46}$H$_{60}$N$_{16}$O$_4$, C 61.31, H 6.71, N 24.87.

trans-[Fe^{II}(L^1)$_2$(NCS)$_2$] (1)

L^1 (20 mg, 0.056 mmol) was dissolved in 3 ml of MeOH. Separately, Fe^{II}(ClO$_4$)$_2$·6H$_2$O (9.8 mg, 0.027 mmol), NaNCS (4.5 mg,

0.056 mmol) and 10 mg ascorbic acid were added to 3 ml MeOH, and the mixture was stirred until all solids were dissolved. The $Fe(NCS)_2$ solution was then added dropwise to the solution containing L^1, and the resultant yellow solution was filtered, and the filtrate placed in an open vessel within a vapour-diffusion chamber containing diethyl ether. X-ray diffraction quality crystals formed over the course of two days, and were isolated *via* filtration. Yield: 6 mg (9.7%). MW: 883.66. IR (ATR cm^{-1} room temperature): 3336 (w), 3066 (w), 2976 (m), 2934 (m), 2871 (w), 2052 (s), 1571 (s), 1501 (s), 1461 (s), 1401 (s), 1376 (s), 1361 (s), 1332 (m), 1282 (s), 1236 (sh), 1181 (s), 1153 (s), 1115 (m), 1087 (s), 1054 (m), 1024 (s), 1011 (s), 983 (s), 891 (s), 817 (m), 777 (s), 756 (s), 673 (s), 632 (m). Microanalysis: % found C 49.06, H 4.11, N 25.04; % calculated for $C_{36}H_{36}Cl_2FeN_{16}S_2$, C 48.93, H 4.11, N 25.

trans-[$Fe^{II}(L^1)_2(NCSe)_2$] (2)

This complex was synthesised in low yield using a similar procedure to that used for compound **1**, except that KNCSe (8.1 mg, 0.056 mmol) was used in place of NaNCS. Yield: 5 mg (18.9%). MW: 977.45. IR (ATR cm^{-1} room temperature): 2976 (w), 2065 (s), 1673 (w), 1566 (s), 1499 (s), 1479 (s), 1468 (s), 1407 (s), 1359 (s), 1334 (s), 1285 (s), 1237 (s), 1181 (s), 1158 (s), 1090 (s), 1055 (s), 1011 (s), 984 (s), 822 (s), 778 (s), 757 (s), 674 (s), 632 (s). Microanalysis: % found C 43.18, H 2.90, N 23.24; % calculated for $C_{36}H_{36}B_2Cl_2FeN_{16}Se_2$, C 44.24, H 3.71, N 22.93.

trans-[$Fe^{II}(L^1)_2(NCBH_3)_2$] (3) and 3·1.5H$_2$O

A similar method was employed to that used for **1** and **2**, but using $Fe^{II}(BF_4)_2$·6H$_2$O (9.1 mg, 0.027 mmol) in place of Fe^{II}-(ClO$_4$)$_2$·6H$_2$O and with NaNCBH$_3$ (3.5 mg, 0.056 mmol) used instead of NaNCS–KNCSe. However, once the precursor solutions had been combined, the solvent was reduced sufficiently to a point where a precipitate formed in solution. The solution was then filtered and the yellow precipitate that was isolated was re-dissolved in a small amount of CHCl$_3$. This CHCl$_3$ solution was placed in an open vessel within a vapour-diffusion chamber containing diethyl ether, giving a small number of yellow crystals of **3** that were suitable for X-ray crystallographic analysis. Yield: 1 mg (4%). The bulk powder (3·1.5H$_2$O) was synthesised as above where the MeOH solvent was reduced in volume forming a yellow precipitate which was isolated *via* filtration. This was then analysed using magnetic susceptibility, infrared, microanalytical, TGA and DSC measurements. MW: 847.20 (anhydrous). IR (ATR cm^{-1} room temperature): 3390(br), 2933 (w), 2326 (m), 2158 (m), 1565 (s), 1500 (s), 1480 (s), 1469 (s), 1407 (s), 1362 (s), 1286 (s), 1241 (s), 1181 (s), 1088 (s), 1023 (s), 985 (s), 823 (s), 797 (s), 779 (s), 759 (s), 675 (s). The microanalysis suggested four solvate waters (% found C 47.18, H 5.00, N 24.24; Cl 7.38% calculated for $C_{36}H_{50}B_2Cl_2FeN_{16}O_4$ (3·4H$_2$O), C 47.04, H 5.48, N 24.38, Cl 7.71) whereas the TGA analysis (Fig. S13†) showed a gradual weight loss of *ca.* 3% between 25 °C and 230 °C, equivalent to the loss of 1.5H$_2$O. The bulk powder sample has been labelled throughout the text as (3·1.5H$_2$O) based on the TGA analysis.

Although the exact number of solvate waters is not known the physical analyses (*vide supra*) are consistent with each other and with that of a hydrated sample.

cis-[$Fe^{II}(L^2)(NCS)_2$]·CH$_2$Cl$_2$ (4)

The L^2 ligand (50 mg, 0.056 mmol) was dissolved in 3 ml of MeOH. Separately, NaNCS (9.2 mg, 0.112 mmol), Fe^{II}-(ClO$_4$)$_2$·6H$_2$O (20.3 mg, 0.056 mmol) and 10 mg ascorbic acid were dissolved in 3 ml of MeOH. The $Fe(NCS)_2$ solution was added dropwise to the solution of L^2, giving a yellow solution, which was filtered. Over time, a precipitate formed, and it was re-dissolved in 3 ml of CH$_2$Cl$_2$ and placed in an open vessel within a vapour diffusion chamber containing diethyl ether. X-ray diffraction quality crystals formed after 1 week, and were isolated *via* filtration. Yield: 20 mg (31%). MW: 1073.09. IR (ATR cm^{-1} room temperature): 3941 (w), 3077 (w), 2971 (w), 2930 (m), 2863 (m), 2059 (s), 1599 (s), 1558 (s), 1507 (s), 1479 (s), 1461 (s), 1433 (s), 1417 (s), 1362 (s), 1330 (s), 1300 (s), 1258 (s), 1233 (s), 1194 (s), 1169 (s), 1154 (s), 1110 (s), 1076 (s), 1060 (s), 1029 (s), 1015 (s), 974 (s), 928 (s), 908 (s), 878 (s), 849 (s), 834 (s), 803 (s), 774 (s), 755 (s), 726 (s), 689 (s), 673 (s), 628 (s). Microanalysis: % found C 50.78, H 5.46, N 21.35; % calculated for $C_{49}H_{62}Cl_2FeN_{18}O_4S_2$ (4·CH$_2$Cl$_2$), C 50.82, H 5.40, N 21.77.

cis-[$Fe^{II}(L^2)(NCSe)_2$]·CH$_2$Cl$_2$ (5)

Compound **5** was synthesised using a similar method to that given for complex **4** but with KNCSe (8.1 mg, 0.056 mmol) used instead of NaNCS. Yield: 28 mg (40%). MW: 1166.87. IR (ATR cm^{-1} room temperature): 3503 (w), 3077 (w), 2970 (m), 2930 (s), 2861 (m), 2360 (w), 2063 (s), 1600 (s), 1558 (s), 1506 (s), 1478 (s), 1462 (s), 1433 (s), 1363 (s), 1330 (s), 1301 (s), 1260 (s), 1235 (s), 1155 (s), 1110 (s), 1060 (s), 1016 (s), 974 (s), 928 (s), 908 (s), 878 (s), 803 (s), 774 (s), 754 (s), 689 (s), 674 (s). Microanalysis: % found C 46.73, H 4.82, N 19.63; % calculated for $C_{49}H_{62}Cl_2FeN_{18}O_4Se_2$ (5·CH$_2$Cl$_2$), C 47.01, H 4.99, N 20.14.

cis-[$Fe^{II}(L^2)(NCBH_3)_2$] (6)

A similar method was employed to that used for **4**, however $Fe^{II}(BF_4)_2$·6H$_2$O (18.8 mg 0.056 mmol) was used instead of $Fe^{II}(ClO_4)_2$·6H$_2$O, and NaNCBH$_3$ (7 mg, 0.112 mmol) used instead of NaNCS. Yield: 15 mg (23%). MW: 1121.56. IR (ATR cm^{-1} room temperature): 2931 (w), 2862 (w), 2347 (m), 2184 (s), 1601 (s), 1570 (s), 1559 (s), 1507 (s), 1481 (s), 1463 (s), 1435 (s), 1417 (s), 1363 (s), 1331 (s), 1300 (s), 1260 (s), 1235 (s), 1156 (s), 1121 (s), 1085 (s), 1062 (s), 1016 (s), 975 (s), 928 (s), 909 (s), 879 (s), 804 (s), 775 (s), 756 (s), 690 (s), 675 (s), 631 (s). Microanalysis: % found C 53.78, H 6.31, N 22.54; % calculated for $C_{49}H_{68}Cl_2FeN_{18}O_4B_2$ (6·CH$_2$Cl$_2$), C 52.47, H 6.11, N 22.48.

trans-[$Fe^{II}(L^3)(NCS)_2$]$_n$ (7)

L^3 (20 mg, 0.018 mmol), $Fe^{II}(BF_4)_2$·6H$_2$O (6.1 mg, 0.018 mmol) and NaNCS (2.9 mg, 0.036 mmol) were dissolved in 3 ml of dimethylformamide and placed in a sealed vial. The tube was heated on a hot-plate and held at 130 °C for 16 h, after which time the vial was left to slowly reach ambient temperature.

Upon cooling, small yellow crystals appeared on the side of the vial.

Yield: 7 mg (30.6%). MW: 1269. IR (ATR cm^{-1} room temperature) 3432 (br), 2866 (m), 2052 (s), 1590 (s), 1552 (s), 1524 (s), 1463 (s), 1407 (s), 1371 (s), 1295 (s), 1265 (s), 1177 (s), 1097 (s), 996 (s), 804 (s), 775 (s), 738 (s), 666 (s). Microanalysis: % found C 56.96, H 4.65, N 24.00; % calculated for $C_{60}H_{56}FeN_{22}O_4S_2$ (7), C 56.78, H 4.45, N 24.28.

trans-[Fe^{II}(L^3)(NCSe)$_2$]$_n$ (8)

L^3 (20 mg, 0.018 mmol), Fe^{II}(BF$_4$)$_2$·6H$_2$O (6.1 mg, 0.018 mmol) and KNCSe (5.2 mg, 0.036 mmol) were dissolved in 3 ml of dimethylformamide and placed in a sealed vial. The tube was heated on a hot-plate and held at 130 °C for 16 h, after which time the vial was allowed to slowly reach ambient temperature. Upon cooling, small yellow crystals appeared on the side of the vial. Yield: 6 mg (24.5%). MW 1363. IR (ATR, cm^{-1}, room temperature) 3443 (br), 2864 (m), 2054 (s), 1591 (s), 1553 (s), 1524 (s), 1464 (s), 1409 (s), 1372 (s), 1295 (s), 1266 (s), 1177 (s), 1097 (s), 997 (s), 805 (s), 775 (s), 744 (s), 666 (s). Microanalysis: % found C 52.04, H 4.05, N 22.36; % calculated for $C_{60}H_{56}FeN_{22}O_4Se_2$, C 52.87, H 4.14, N 22.61.

X-ray crystallography

X-ray crystallographic measurements on **2** and **6** were performed at 173(2) K (**2**) and 123(2) K (**6**) using a Bruker Smart Apex X8 diffractometer with Mo Kα radiation, $\lambda = 0.71073$ Å. Single crystals were mounted on a glass fibre using oil. The data collection and integration were performed within SMART and SAINT+ software programs, and corrected for absorption using the Bruker SADABS program.[42] X-ray crystallographic

measurements on **4** and **5** were performed at 173(2) K on a Enraf-Nonius Kappa CCD with Mo Kα radiation, $\lambda = 0.71073$ Å. X-ray data were processed using the DENZO program[43] and data was corrected for absorption using the SORTAV package.[44] X-Ray measurements were performed at 100(2) K for **1**, **3**, **7** and **8** at the Australian Synchrotron MX2 beam-line. The data collection and integration were performed within Blu-Ice[45] and XDS[46] software programs. Crystallographic data and refinement parameters for **1–8**, given in Tables 2 and 3, were solved by direct methods (SHELXS-97), and refined (SHELXL-97) by full least-squares on all F^2 data.[47] All other non-hydrogen atoms in **1–8** were refined anisotropically and all hydrogen atoms were placed in calculated positions. Residual electron density located above the crown moiety in complexes **4** and **5** was unable to be assigned unambiguously and so was treated with SQUEEZE[48] which suggested a relatively small amount of electron density (4.5 e per complex for **4**, 6.5 e per complex for **5**). This is in contrast to the microanalysis which suggests the presence of a single dichloromethane molecule. CCDC numbers 883899–883904 (**1** to **6**), 945424 (**7**) and 945423 (**8**).

Physical measurements

Elemental analyses (C, H, N) were performed by the Campbell Microanalytical Laboratory, University of Otago, Dunedin, New Zealand. Infrared spectra were recorded on a Bruker Opus/IR IFS 55 spectrophotometer in a range 4000–400 cm^{-1}. Differential scanning calorimetry (DSC) was performed on a DSC Q100 series from TA instruments with 4–5 mg of sample in closed aluminium pans, at a ramp rate of 5 K per minute. Two cooling–heating cycles were performed where complex **3** was

Table 2 Crystallographic details for complexes **1–6**

	1	2	3	4	5	6
Formula	$C_{36}H_{36}Cl_2FeN_{16}S_2$	$C_{36}H_{36}Cl_2FeN_{16}Se_2$	$C_{36}H_{42}Cl_2FeN_{16}B_2$	$C_{48}H_{60}FeN_{18}O_4S_2$	$C_{48}H_{60}FeN_{18}O_4Se_2$	$C_{49}H_{68}B_2Cl_2FeN_{18}O_4$
FW (g mol^{-1})	883.68	977.48	847.23	1073.11	1166.91	1121.58
T (K)	100	173	123	173	173	123
Crystal system	Monoclinic	Monoclinic	Monoclinic	Orthorhombic	Orthorhombic	Orthorhombic
Space group	$P2_1/n$	$P2_1/n$	$P2_1/n$	$Pbcn$	$Pbcn$	$Pbcn$
Z	2	2	2	4	4	4
a (Å)	10.151(2)	10.336(1)	10.664(2)	16.646(3)	16.781(3)	16.657(1)
b (Å)	16.530(3)	16.467(2)	16.148(3)	19.181(4)	19.268(4)	19.263(1)
c (Å)	12.110(2)	12.172(1)	11.932(2)	17.078(3)	17.107(3)	16.898(1)
α (°)	90	90	90	90	90	90
β (°)	105.50(3)	104.658(3)	101.77(3)	90	90	90
γ (°)	90	90	90	90	90	90
V (Å^3)	1958.1(7)	2004.1(3)	2011.5(7)	5452.9(19)	5531.3(19)	5422.1(4)
ρ_{calc} (g cm^{-3})	1.499	1.620	1.399	1.307	1.401	1.374
μ (mm^{-1})	0.680	2.377	0.558	0.413	1.648	0.439
Measured/ independent (R_{int}) reflections	24 043/3254 (0.0386)	12 951/4591 (0.0732)	14 356/4022 (0.0667)	37 799/6906 (0.1000)	20 679/6673 (0.1338)	53 578/6221 (0.0870)
Observed reflections [$I > 2\sigma(I)$]	3062	2608	3081	4418	3035	4372
$R_1{}^a$, w$R_2{}^b$ [$I > 2\sigma(I)$]	0.0645, 0.1923	0.0532, 0.0844	0.1213, 0.2990	0.0648, 0.1567	0.0855, 0.1813	0.0676, 0.1839
R_1, wR_2 (all data)	0.0668, 0.1936	0.1216, 0.1034	0.1448, 0.3176	0.1108, 0.1751	0.1933, 0.2171	0.0984, 0.2049
Goodness-of-fit on F^2	1.161	0.971	1.052	1.075	0.946	1.045

$^a R_1 = \sum||F_o| - |F_c||/\sum|F_o|$. ^{b} w$R_2 = \{\sum[w(F_o{}^2 \sum F_c{}^2)^2]/\sum[w(F_o{}^2)]\}^{1/2}$.

Table 3 Crystallographic details for complexes **7** and **8**

	7	8
Formula	$C_{60}H_{56}Fe_1N_{22}O_4S_2$	$C_{60}H_{56}Fe_1N_{22}O_4Se_2$
FW (g mol⁻¹)	1269.24	1363.04
T (K)	100 (2)	100 (2)
Crystal system	Triclinic	Triclinic
Space group	$P\bar{1}$	$P\bar{1}$
Z	1	1
a (Å)	10.486(2)	10.620(2)
b (Å)	12.423(3)	12.570(3)
c (Å)	13.133(3)	13.150(3)
α (°)	71.52(3)	70.65(3)
β (°)	72.10(3)	71.26(3)
γ (°)	66.56(3)	65.99(3)
V (Å³)	1456.0(5)	1477.2(5)
ρ_{calc} (g cm⁻³)	1.448	1.532
μ (mm⁻¹)	0.401	1.557
Measured/independent	56 483, 8096	46 822, 6541
(R_{int}) reflections	(0.0509)	(0.0588)
Observed reflections [$I > 2\sigma(I)$]	7449	5450
R_1 [a], wR_2 [b] [$I > 2\sigma(I)$]	0.0508, 0.1340	0.0476, 0.1286
R_1, wR_2 (all data)	0.0543, 0.1382	0.0581, 0.1356
Goodness-of-fit on F^2	1.050	1.040

[a] $R_1 = \sum ||F_o| - |F_c||/\sum |F_o|$. [b] w$R_2 = \{\sum[w(F_o{}^2 \sum F_c{}^2)^2]/\sum[w(F_o{}^2)]\}^{1/2}\}^{1/2}$.

cooled to 123 K, held for 3 minutes and heated to 273 K. Thermal scans below room temperature were calibrated *via* the cyclohexane solid–solid transition (186.1 K, 6.70 kJ mol⁻¹) and melting point (279.7 K, 2.63 kJ mol⁻¹). Transition temperatures are reported using the peak maximum of the thermal transition. Temperature values were determined with a ±4.8 K accuracy and enthalpy scans were estimated with an experimental uncertainty of ±12% for a scan rate of 10 K min⁻¹.

Variable temperature solid state direct current (dc) magnetic susceptibility data down to 5 K were collected with an applied field of 0.5 T on a Quantum Design MPMS 5 T magnetometer calibrated by use of a standard palladium sample (Quantum Design) of accurately known magnetisation or by use of magnetochemical calibrants such as $CuSO_4 \cdot 5H_2O$. Microcrystalline samples were dispersed in Vaseline to avoid torquing of the crystallites. The sample mulls were contained in a calibrated capsule held at the centre of a drinking straw that was fixed at the end of the sample rod.

Photomagnetic characterisation for compounds **5** and **6** were carried out at CNRS, Université de Bordeaux, ICMCB, with a Spectrum Physics Series 2025 Kr+ laser coupled through an optical fibre into the cavity of the MPMS-55 Quantum design SQUID magnetometer operating at 2 T. Samples were prepared as a thin layer (*ca.* 0.1 mg) to promote full penetration of the irradiated light. The sample weight was obtained by comparing its thermal spin transition behaviour with an accurately weighed sample.[38] The sample was first slowly cooled to 10 K by ensuring that potential trapping of HS species at low temperatures did not occur. Irradiation to photosaturation was carried out a number of times at different wavelengths to determine which source was most efficient at a power intensity of 5 mW cm⁻² (to prevent warming of the sample). Samples were then cooled to 10 K and irradiated with

green light (λ = 532 nm at 5 mW cm⁻² was found to be the most efficient) until photosaturation was reached. Then, in the absence of irradiation, the temperature was increased at a rate of 0.3 K min⁻¹. The extreme of the $\delta\chi_M T/\delta T$ *vs. T* plot gave the T(LIESST) values for compounds **5** and **6**, defined as the temperature for which the light-induced HS information is erased.[38] At 10 K, compounds **5** and **6** were again irradiated to photosaturation, and in the absence of irradiation the relaxation kinetics at 35, 40, 45, 47.5 and 50 K were measured for compound **6**;. The relaxation kinetics were measured at 10, 20, 45, 50, 54, 56, 60, 65, 70 and 75 K for **5**. See ESI† for further details.

^{1}H NMR and ^{13}C NMR spectra were recorded on a Bruker DPX 200 MHz, Bruker Avance 400 MHz and a Varian Inova 500 MHz. Electrospray ionization mass spectra (ESI-MS) were recorded with a Micromass (now Waters) ZMD with Waters alliance e2695 HPLC system for automatic sample injections. MeOH was the mobile phase and had a flow rate of 100 μL min⁻¹.

Notes and references

1 See spin crossover articles by various authors in: (*a*) *Spin-crossover in Transition metal compounds*, ed. P. Gütlich and H. A. Goodwin, *Top. Curr. Chem.*, Springer, Berlin, 2004, pp. 233–235; (*b*) *Spin Crossover Materials. Properties and Applications*. ed. M. A. Halcrow, Wiley, London, 2013; (*c*) Cluster issue "Spin Crossover Complexes". *Eur. J. Inorg. Chem.*, 2013, 573–1067.

2 (*a*) P. Gütlich, Y. Garcia and H. A. Goodwin, *Chem. Soc. Rev.*, 2004, **29**, 419–427; (*b*) O. Kahn, *Nature*, 1999, **21**, 319.

3 K. S. Murray and C. J. Kepert, *Top. Curr. Chem.*, 2004, **233**, 195.

4 (*a*) M. Yamada, M. Ooidemizu, Y. Ikuta, S. Osa, N. Matsumoto, S. Iijima, M. Kojima, F. Dahan and J.-P. Tuchagues, *Inorg. Chem.*, 2003, **42**, 8406; (*b*) G. S. Matouzenko, G. Molnar, N. Brefuel, M. Perrin, A. Bousseksou and S. A. Borshch, *Chem. Mater.*, 2003, **15**, 550; (*c*) Y. Ikuta, M. Ooidemizu, Y. Yamahata, M. Yamada, S. Osa, N. Matsumoto, S. Iijima, Y. Sunatsuki, M. Kojima, F. Dahan and J.-P. Tuchagues, *Inorg. Chem.*, 2003, **42**, 7001; (*d*) Y. Sunatsuki, Y. Ikuta, N. Matsumoto, H. Ohta,

M. Kojima, S. Iijima, S. Hayami, Y. Maeda, S. Kaizaki, F. Dahan and J.-P. Tuchagues, *Angew. Chem., Int. Ed.*, 2003, **42**, 1614; (*e*) B. Weber, W. Bauer, T. Pfaffeneder, M. M. Dîrtu, A. D. Naik, A. Rotaru and Y. Garcia, *Eur. J. Inorg. Chem.*, 2011, 3193.

5 (*a*) J. F. Lètard, P. Guionneau, E. Codjovi, O. Lavastre, G. Bravic, D. Chasseau and O. Kahn, *J. Am. Chem. Soc.*, 1997, **119**, 10861; (*b*) S. Hayami, Z.-Z. Gu, M. Shiro, Y. Einaga, A. Fujishima and O. Sato, *J. Am. Chem. Soc.*, 2000, **122**, 7126; (*c*) R. Boča, M. Boča, L. Dlháň, M. Vrbova and R. Werner, *Inorg. Chem.*, 2001, **40**, 3025; (*d*) J. A. Real, B. Gallois, T. Granier, F. Suez-Panama and J. Zarembowitch, *Inorg. Chem.*, 1992, **31**, 4972; (*e*) Z.-J. Zhong, J.-Q. Tao, Z. Yu, C.-Y. Duan, Y.-J. Liu and X.-Z. You, *J. Chem. Soc., Dalton Trans.*, 1998, 327; (*f*) M. A. Halcrow, *Chem. Soc. Rev.*, 2011, **40**, 4119.

6 (*a*) S. Arata, H. Torigoe, T. Iihoshi, N. Matsumoto, F. Dahan and J.-P. Tuchagues, *Inorg. Chem.*, 2005, **44**, 9288; (*b*) D. L. Reger, J. R. Gardinier, W. R. Gemmil, M. D. Smith, A. M. Shahin, G. J. Long, L. Rebbouh and F. Grandjean, *J. Am. Chem. Soc.*, 2005, **127**, 2303.

7 (*a*) Y. Garcia, V. Niel, M. C. Muňov and J. A. Real, *Top. Curr. Chem.*, 2004, **233**, 229, Springer, Berlin; (*b*) J. A. Real, A. B. Gaspar, V. Niel and M. C. Muňov, *Coord. Chem. Rev.*, 2003, **236**, 121.

8 (*a*) C. Faulmann, K. Jacob, S. Dorbe, S. Lampert, I. Malfant, M.-L. Doublet, L. Valade and J. A. Real, *Inorg. Chem.*, 2007, **46**, 8548; (*b*) K. Takahashi, H.-B. Cui, Y. Okano, H. Kobayashi, H. Mori, H. Tajima, Y. Einaga and O. Sato, *J. Am. Chem. Soc.*, 2008, **130**, 6688.

9 (*a*) G. J. Halder, C. J. Kepert, B. Moubaraki, K. S. Murray and J. D. Cashion, *Science*, 2002, **298**, 1762; (*b*) S. M. Neville, G. J. Halder, K. W. Chapman, M. B. Duriska, P. D. Southon, J. D. Cashion, J.-F. Létard, B. Moubaraki, K. S. Murray and C. J. Kepert, *J. Am. Chem. Soc.*, 2008, **130**, 2869; (*c*) S. M. Neville, G. J. Halder, K. W. Chapman, M. B. Duriska, B. Moubaraki, K. S. Murray and C. J. Kepert, *J. Am. Chem. Soc.*, 2009, **131**, 12106.

10 (*a*) Y. Sunatsuki, Y. Ikuta, N. Matsumoto, H. Ohta, M. Kojima, S. Iijima, S. Hayami, Y. Maeda, S. Kaizaki, F. Dahan and J.-P. Tuchagues, *Angew. Chem., Int. Ed.*, 2003, **42**, 1614; (*b*) M. Clemente-León, E. Coronado, M. López-Jordà and J. C. Waerenborgh, *Inorg. Chem.*, 2011, **50**, 9122.

11 R. Carballo, B. Covelo, E. M. Vázquez-López, E. Garciá-Martinez, A. Castineiras and C. Janiak, *Z. Anorg. Allg. Chem.*, 2005, **631**, 2006.

12 J. Y. Lu, T. J. Schroeder, A. M. Babb and M. Olmstead, *Polyhedron*, 2001, **20**, 2445.

13 P. Cortés, A. M. Atria, M. T. Garland and R. Baggio, *Acta Crystallogr., Sect. C: Cryst. Struct. Commun.*, 2006, **62**, m297.

14 M. Quesada, P. de Hogg, P. Gamez, O. Roubeau, G. Aromi, B. Donnadieu, C. Massera, M. Lutz, A. L. Spek and J. Reedijk, *Eur. J. Inorg. Chem.*, 2006, 1353.

15 J. J. M. Amoore, C. J. Kepert, J. D. Cashion, B. Moubaraki, S. M. Neville and K. S. Murray, *Chem.–Eur. J.*, 2006, **12**, 8220.

16 M. Quesada, V. A. de la Pena-O'Shea, G. Aromí, S. Geremia, C. Massera, O. Roubeau, P. Gamez and J. Reedijk, *Adv. Mater.*, 2007, **19**, 1397.

17 S. M. Neville, B. A. Leita, D. A. Offermann, M. B. Duriska, B. Moubaraki, K. W. Chapman, G. J. Halder and K. S. Murray, *Eur. J. Inorg. Chem.*, 2007, 1073.

18 S. M. Neville, B. A. Leita, G. J. Halder, C. J. Kepert, B. Moubaraki, J.-F. Létard and K. S. Murray, *Chem.–Eur. J.*, 2008, **14**, 10123.

19 Y. Maeda, M. Suzuki, S. Hirose, S. Hayami, T. Oniki and S. Sugihara, *Bull. Chem. Soc. Jpn.*, 1998, **71**, 2837.

20 T. M. Ross, B. Moubaraki, S. M. Neville, S. R. Batten and K. S. Murray, *Dalton Trans.*, 2012, **41**, 1512.

21 M. B. Duriska, S. M. Neville and S. R. Batten, *Chem. Commun.*, 2009, 5579.

22 I. A. Gass, S. R. Batten, C. M. Forsyth, B. Moubaraki, C. J. Schneider and K. S. Murray, *Coord. Chem. Rev.*, 2011, **255**, 2058.

23 T. M. Ross, B. Moubaraki, K. S. Wallwork, S. R. Batten and K. S. Murray, *Dalton Trans.*, 2011, **40**, 10147.

24 T. J. Mooibroek, S. J. Teat, C. Massera, P. Gamez and J. Reedijk, *Cryst. Growth Des.*, 2006, **6**, 1569.

25 P. Guionneau, M. Marchivie, G. Bravic, J.-F. Létard and D. Chasseau, *Top. Curr. Chem.*, 2004, **234**, 97.

26 K. S. Murray, in *Spin Crossover Materials. Properties and Applications*, ed. M. A. Halcrow, Wiley, London, 2013, ch. 1.

27 C. Carbonera, C. A. Kilner, J. F. Lètard and M. A. Halcrow, *Dalton Trans.*, 2007, 1284.

28 A. Bousseksou, G. Molnár, L. Salmon and W. Nicolazzi, *Chem. Soc. Rev.*, 2011, **40**, 3313.

29 C. P. Slichter and H. P. Drickamer, *J. Chem. Phys.*, 1972, **56**, 2142.

30 A. V. Sinitskiy, A. L. Tchougréeff and R. Dronskowski, *Phys. Chem. Chem. Phys.*, 2011, **13**, 13238.

31 (*a*) M. Kepenekian, B. Le Guennic and V. Robert, *Phys. Rev. B: Condens. Matter*, 2009, **79**, 094428; (*b*) M. Kepenekian, B. Le Guennic and V. Robert, *J. Am. Chem. Soc.*, 2009, **131**, 11498; (*c*) M. Kepenekian, J. S. Costa, B. Le Guennic, P. Maldivi, S. Bonnet, J. Reedijk, P. Gamez and V. Robert, *Inorg. Chem.*, 2010, **49**, 11057.

32 J. A. Real, H. Bolvin, A. Bousseksou, A. Dworkin, O. Kahn, F. Varret and J. Zarembowitch, *J. Am. Chem. Soc.*, 1992, **114**, 4650.

33 (*a*) K. Nakano, N. Suemura, S. Kawata, A. Fuyuhiro, T. Yagi, S. Nasu, S. Morimoto and S. Kaizaki, *Dalton Trans.*, 2004, 982; (*b*) K. Nakano, N. Suemura, K. Yoneda, S. Kawata and S. Kaizaki, *Dalton Trans.*, 2005, 740.

34 L. Capes, J. F. Lètard and O. Kahn, *Chem.–Eur. J.*, 2000, **6**, 2246.

35 (*a*) S. Grimme, J. Antony, S. Ehrlich and H. Krieg, *J. Chem. Phys.*, 2010, **132**, 154104; (*b*) S. Grimme, *J. Comput. Chem.*, 2006, **27**, 1787.

36 (*a*) A. Schäfer, H. Horn and R. Ahlrichs, *J. Chem. Phys.*, 1992, **97**, 2571; (*b*) A. Schäfer, C. Huber and R. Ahlrichs, *J. Chem. Phys.*, 1994, **100**, 5829.

37 M. J. Frisch, G. W. Trucks, H. B. Schlegel, G. E. Scuseria, M. A. Robb, J. R. Cheeseman, G. Scalmani, V. Barone, B. Mennucci, G. A. Petersson, H. Nakatsuji, M. Caricato, X. Li, H. P. Hratchian, A. F. Izmaylov, J. Bloino, G. Zheng, J. L. Sonnenberg, M. Hada, M. Ehara, K. Toyota, R. Fukuda, J. Hasegawa, M. Ishida, T. Nakajima, Y. Honda, O. Kitao, H. Nakai, T. Vreven, J. A. Montgomery Jr., J. E. Peralta, F. Ogliaro, M. Bearpark, J. J. Heyd, E. Brothers, K. N. Kudin, V. N. Staroverov, R. Kobayashi, J. Normand, K. Raghavachari, A. Rendell, J. C. Burant, S. S. Iyengar, J. Tomasi, M. Cossi, N. Rega, J. M. Millam, M. Klene, J. E. Knox, J. B. Cross, V. Bakken, C. Adamo, J. Jaramillo, R. Gomperts, R. E. Stratmann, O. Yazyev, A. J. Austin, R. Cammi, C. Pomelli, J. W. Ochterski, R. L. Martin, K. Morokuma, V. G. Zakrzewski, G. A. Voth, P. Salvador, J. J. Dannenberg, S. Dapprich, A. D. Daniels, O. Farkas, J. B. Foresman, J. V. Ortiz, J. Cioslowski and D. J. Fox, *GAUSSIAN 09 (Rev. A.02)*, Gaussian, Inc., Wallingford, CT, 2009.

38 J.-F. Létard, *J. Mater. Chem.*, 2006, **16**, 2550.

39 M. Marchivie, P. Guionneau, J.-F. Létard and D. Chasseau, *Acta Crystallogr., Sect. B: Struct. Sci.*, 2005, **61**, 25.

40 Y. B. Go, X. Wang, E. V. Anokhina and A. J. Jacobson, *Inorg. Chem.*, 2005, **44**, 8265.

41 T. Hermon and E. Y. Tshuva, *J. Org. Chem.*, 2008, **73**, 5953.

42 G. M. Sheldrick, *SADABS, Program for area detector adsorption correction*, Institute for Inorganic Chemistry, University of Göttingen, Germany, 1996.

43 Z. Otwinowski and W. Minor, *Methods Enzymol.*, 1997, **276**, 307.

44 R. H. Blessing, *J. Appl. Crystallogr.*, 1997, **30**, 421.

45 T. M. McPhillips, S. E. McPhillips, H. J. Chiu, A. E. Cohen, A. M. Deacon, P. J. Ellis, E. Garman, A. Gonzalez, N. K. Sauter, R. P. Phizackerley, S. M. Soltis and P. Kuhn, Blu-Ice and the Distributed Control System: software for data acquisition and instrument control at macromolecular crystallography beamlines, *J. Synchrotron Radiat.*, 2002, **9**, 401.

46 W. Kabsch, *J. Appl. Crystallogr.*, 1993, **26**, 795.

47 (*a*) G. M. Sheldrick, *SHELXL-97, Program for refinement of crystal structures*, University of Göttingen, Germany, 1997; (*b*) A. L. Spek, *Acta Crystallogr., Sect. A: Fundam. Crystallogr.*, 1990, **46**, C34.

48 A. L. Spek, *J. Appl. Crystallogr.*, 2003, **36**, 7.